1965

The development of conical stress forms by explosive charges

Walter T. Casquino

THE DEVELOPMENT OF CONICAL STRESS FORMS BY EXPLOSIVE CHARGES

BY

WALTER T. CASQUINO

A

THESIS

submitted to the faculty of the

UNIVERSITY OF MISSOURI AT ROLLA

in partial fulfillment of the requirements for the

Degree of

MASTER OF SCIENCE IN MINING ENGINEERING

Rolla, Missouri

1965

Approved by

Richard L. Ash (Advisor) Gerard B. Rupert

Albert M. Koehler Yolan B. Aughenbaugh

ABSTRACT

Usually stresses generated by explosive charges during blasting are considered to propagate through materials in a spherical manner. Although conical stress waves had been suggested by a few investigators they have never been clearly defined or studied in the laboratory.

An experimental technique using models was developed to produce conical stress waves from an explosive. Several materials with different properties were selected as models for the purpose of determining whether or not conical waves could be generated in all materials.

This investigation showed that conical stress waves do exist under certain conditions, which would closely approximate those present for much of field blasting. The angle of the developed stress cone was found to directly affect the shape of craters produced. In addition, the minimum angle of incidence for the stresses impinging on accoustical interfaces was defined by that angle.

ACKNOWLEDGEMENTS

The author wishes to express his sincere gratitude for the assistance given him during the conduct of this investigation. Special recognition is due to the Organization of American States for giving him the opportunity to pursue graduate study, to members of the Department of Mining and Petroleum Engineering at the University of Missouri at Rolla for their help and understanding, and to Professor Richard L. Ash for his competent guidance throughout the period of attendance at the University.

TABLE OF CONTENTS

APPENDICES Page

LIST OF FIGURES

LIST OF TABLES

LIST OF PLATES

I. INTRODUCTION

Cratering relationships derived from confined concentrical explosive charges acting toward one free face serve as the basis for the design of all blasting rounds (1 through 17). However, end-initiated cylindrical explosive charges with a large length-to-diameter ratio (L/D) and bounded by two or more free faces account for the great majority of industrial blasting. Charges with L/D ratios from 20 to as high as 200 are commonly used in both surface and underground blasting. Although the general mechanisms of cratering and fracturing of rock by spherical charges are now fairly well understood, there is almost no information available regarding the influence of charge elongation and multiple free-face geometry on the blasting processes. Past studies have been restricted to L/D ratios below 10, with most cases having ratios less than 6. It was the purpose of this investigation, therefore, to observe the cratering processes of end-initiated long cylindrical charges with L/D ratios in excess of 10, typical of most bench and underground blasting ratios.

In order to isolate each variable factor, a laboratory study was assumed to be best for yielding the greatest amount of reliable data. In-situ testing necessarily would require reasonably large scale blasts, would be expensive to conduct, and would yield results that might be questionable from the viewpoint of reproducability. It would be very difficult, and impossible in many instances, to accurately analyze fracture patterns, shapes and thicknesses of fragments, crater geometries, and stress wave forms under field testing conditions. It was felt imperative that wave form characteristics should be closely

studied, in the event blast effects from the cylindrical charges differed markedly from those predicted by the concentric charge relationships.

High-Velocity Mild Detonating Fuse of 10 and 20-grain strengths were chosen for the explosive charges. The fuse was specially adaptable because of its very small critical diameter, comparative ease and safety in handling, high energy release, and reliability for sustaining a uniform reaction velocity over long charge lengths.

To investigate the influence of materials' properties on crater formation, a cement mortar, Hydrostone, and the nonhomogeneous Jefferson City Dolomite were selected. All of the materials were easily cut, or formed, into specimens. In addition, the drilling of holes for charges in the size desired, i.e., approximately 1/8-inch, offered no difficulty. The materials chosen provided a wide range of densities, Poisson's ratios, propagation velocities, strengths, and textural properties. Studies with Plexiglas, however, were restricted to observe idealized stress patterns, since its properties were very different from rock-like materials. Because this investigation was qualitative, only sonic properties of materials were considered; although certain static properties are used in this thesis for illustrative purposes.

II. CRATERS AND THEIR FORMATION

Cratering is that process by which a bowl-shaped depression is formed by the removal of materials from a mass due to the application of impulsive loads. Craters may also be formed by subsidence. The fundamental action peculiar to crater formation by explosions and the impact of projectiles involves two related processes in competent materials: fracturing of the mass and ejection of the broken material (11, 12, 14, 17, 18, 19, 20).

The size and shape of craters are controlled largely by the magnitude and manner in which the energy sources are applied, the materials' properties, and the geometric relationships between the energy source (or sources) and free (open) surfaces of a medium. Certain aspects of the cratering processes have not yet been clearly defined, e.g., the amount of effective work attributed solely to shock effects, on the one hand, and that due to the gaseous expansion forces, on the other.

A. Basic Crater Forms.

Of the possible crater shapes, only two basic types can be produced: the inverted cone and the trough-like composite crater (Fig. 1). The first type is characteristic of the confined concentric charge and the low L/D ratio cylindrical charge. As a general rule, the included angles a and b, measured from a line perpendicular to a free face and the sides of the crater formed, are considered to be approximately 45 degrees (Fig. 2). Yet, in actual practice angles other than 45 degrees frequently result, for reasons as not yet

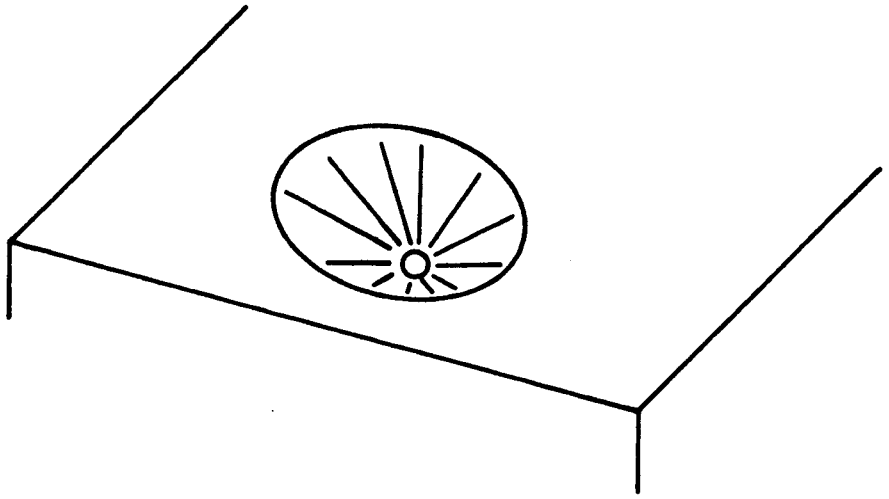

a. Inverted-Cone Crater, One Free Face

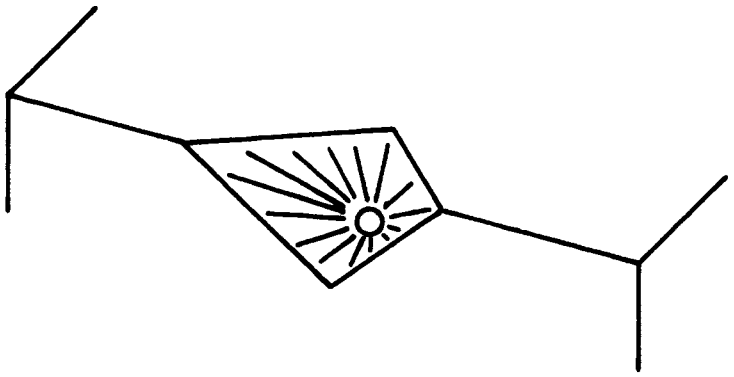

b. Inverted-Cone Crater, Two Free Faces

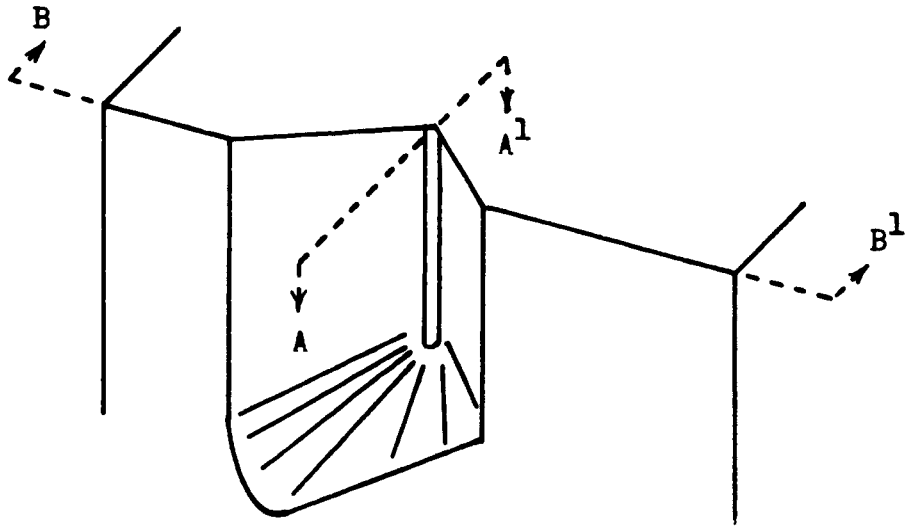

c. Composite Crater, Two Free Faces

Figure 1. Crater Shapes for One and Two Free Faces.

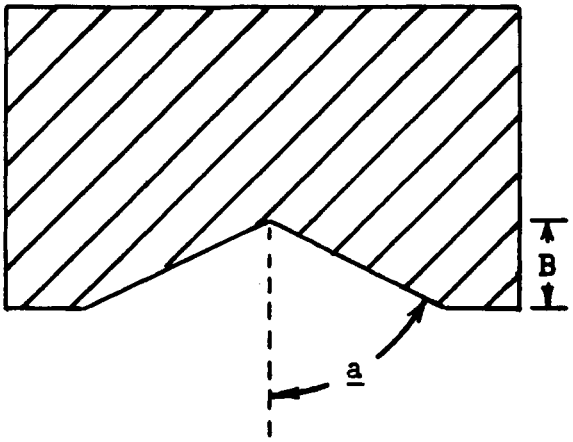

a. Plan View, Section A - A^1

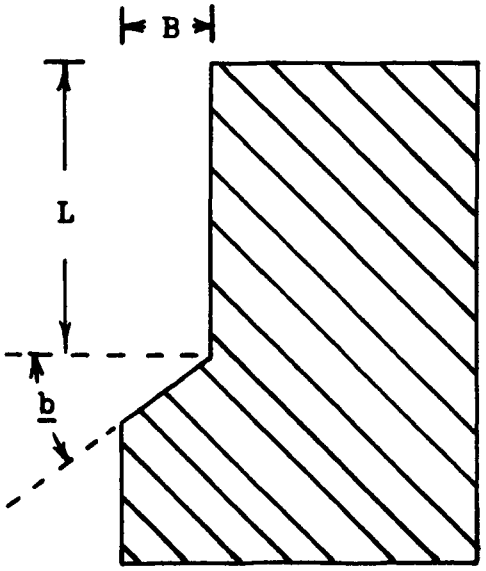

b. Vertical View, Section B - B^1

Figure 2. Crater Parameters for Composite Crater.

fully understood. In the case where a row of equally-spaced, confined point charges are employed, interactions between adjacent charges may combine to develop a trough, or composite crater (13, 14, 20, 21). This latter crater will also develop from the continuous-column charge, i.e., long cylinder, providing the column and series of point charges are aligned parallel to the same free face.

The loading mechanism from the column charge differs from that of the series of point charges in that each segment functions as an independent point source of energy, which releases forces with respect to adjacent points at a finite rate in a continuous time-sequence. The initiation-timing arrangement between the separate point charges of a series may not be related similarly, so that an entirely different effect could be produced. For the row point charges to develop a crater similar to that from the continuous column charge, the former must be properly spaced and initiated at time intervals similar to the time of reaction travel over the same spacing distance in the column charge.

B. Crater Mechanisms.

The stresses induced by impulse-type loading from confined explosive-charges, when propagated to impedance discontinuities must be of adequate strength to initiate fractures for the production of a crater. Since the mechanisms of stress propagation and fracturing have been reported extensively in the literature, a detailed review need not be included in this discussion (10, 13, 14, 19, 23 through 52). But for purpose of clarification relative to this investigation certain fundamental points should be mentioned.

A distinction between the concentric charge and the cylindrical charge with a high L/D ratio is that different types of wave-forms are developed from energy transmission by the explosive into a surrounding medium. The classical assumption is that a spherical compressive wave would be formed in the material. However, it would be incorrect to assume that the cylindrical charge with a large L/D ratio produces either a spherical wave or one that is truly cylindrical in shape. Only in those instances where charges have a relatively low L/D ratio and are initiated at their center, or where the explosive's velocity equals or is less than the wave propagation velocity of the media, could stress waves produced in materials approach that of a spherical form. Also, for the cylindrical wave to be formed, i.e., parallel to the charge length, it would be necessary that all segments in the column initiate simultaneously, which is quite impossible. Thus, and end-initiated cylindrical charge with a reaction velocity exceeding the wave velocity of the medium being blasted would be expected to produce a conical wave form (Fig. 3), having its apex in the direction towards which the explosive reaction propagated along the column (1, 15, 18, 53, 54, 55). In certain instances a symmetrical cone may not be developed from the long cylindrical charge, particularly when composed of blasing agents and used under critical conditions, because the agents may not exhibit steady reaction rates (18, 56). If the reaction velocity varied, stress levels and times of application to the medium also would vary, producing erratic transfers of energy.

In regard to the exact mechanisms responsible for crater formation from blasting, investigators have found that it does not consist only of a simple slabbing action as frequently suggested.

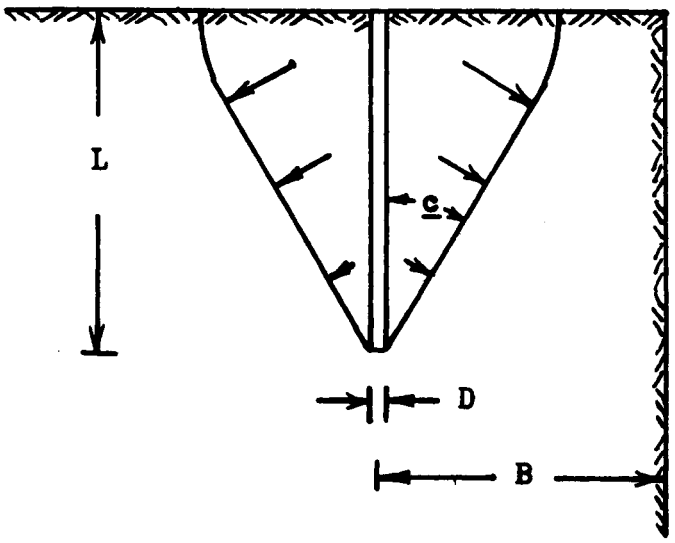

a. Vertical View

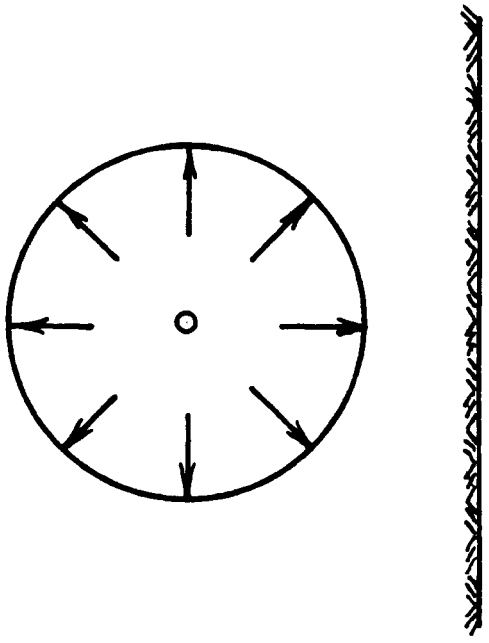

b. Plan View at Top Free Surface

Figure 3. Position of Conical Wave Form Generated by End-Initiated Cylindrical Charge at Completion of Detonation (L/D = 24).

When fracturing begins by an initial scabbing, or slabbing, the extent is usually quite limited. The bulk of cratering appears to result from a stress-release action of rock under strain within the interior of the crater zone. For the case of low-velocity explosives, where initial shock effects may be weak, or even completely absent, there would be no slabbing whatsoever. Properties of the explosives and materials appear to strongly influence whether or not the formation of a crater will be influenced more by the explosive detonation or by the gaseous expansion effects (4, 17, 18, 19, 20, 26, 31, 57, 58, 59).

To make a critical analysis of crater formation processes from long cylindrical charges, the mechanisms by which fractures are initiated must be considered first. In this respect, it is generally believed that the mechanisms occur as the direct result of quickly applied high pressures from the explosive's reaction. In turn, the elastic nature of most rigid materials tend to favor the development and subsequent propagation of two basic kinds of body motions in the materials, in the forms of compressional (P) and shear (S) elastic waves. Theory states that the velocities of propagation for the two waves are related to one another dependent on the material's Poisson's ratio, μ, according to the following relationship (29, 31, 33, 45):

$$V_p = V_s \left[(2-2\mu)/(1-2\mu)\right]^{0.5}. \qquad (1)$$

Providing μ does not exceed or equal the theoretical maximum value of 0.5, or is negative, the P-wave velocity, V_p, always exceeds that of the S-wave, V_s. The following examples illustrate several possibilities:

$$V_p = 2.45\ V_s \text{ when } \mu = 0.40,$$

$$V_p = 1.98\ V_s \text{ when } \mu = 0.33,$$

$$V_p = 1.73\ V_s \text{ when } \mu = 0.25,$$
$$V_p = 1.50\ V_s \text{ when } \mu = 0.10.$$

It can be assumed, therefore, that for most practical conditions involving blasting, the stresses arriving first at points in distance from the energy source would be those propagated by the compressional or P-waves.

When a P-wave strikes a boundary between two different media, there may be as much as four different stress types generated at each point along the wave, two in reflection and two in refraction (Fig. 4). The factors that control the number of stresses generated, their magnitudes and their directions, are the specific angles of incidence, α, of the stress pulses at each point in the wave front and the characteristic accoustical impedance, z, of the two materials at the media boundary. In the case of a rock-to-air interface, there would be little or no stress energy refracted into the air, if its impedance was considered to be zero. This situation would closely approximate the boundary conditions for most field blasting, so that only the reflected stresses are considered by most analysts.

Development of expressions relating the respective amplitudes (or levels) of the reflected P and S stresses in terms of the initial compressive P-wave and angle of incidence, α, is possible on the basis of common relationships found in the literature (29, 31, 45, 57). By substitution, utilizing Formula 1, above, and Snell's Law, where $\sin \alpha_s = V_s \sin \alpha / V_p$, in which α_s is the angle of the reflected S-pulse, the expressions would be as follows:

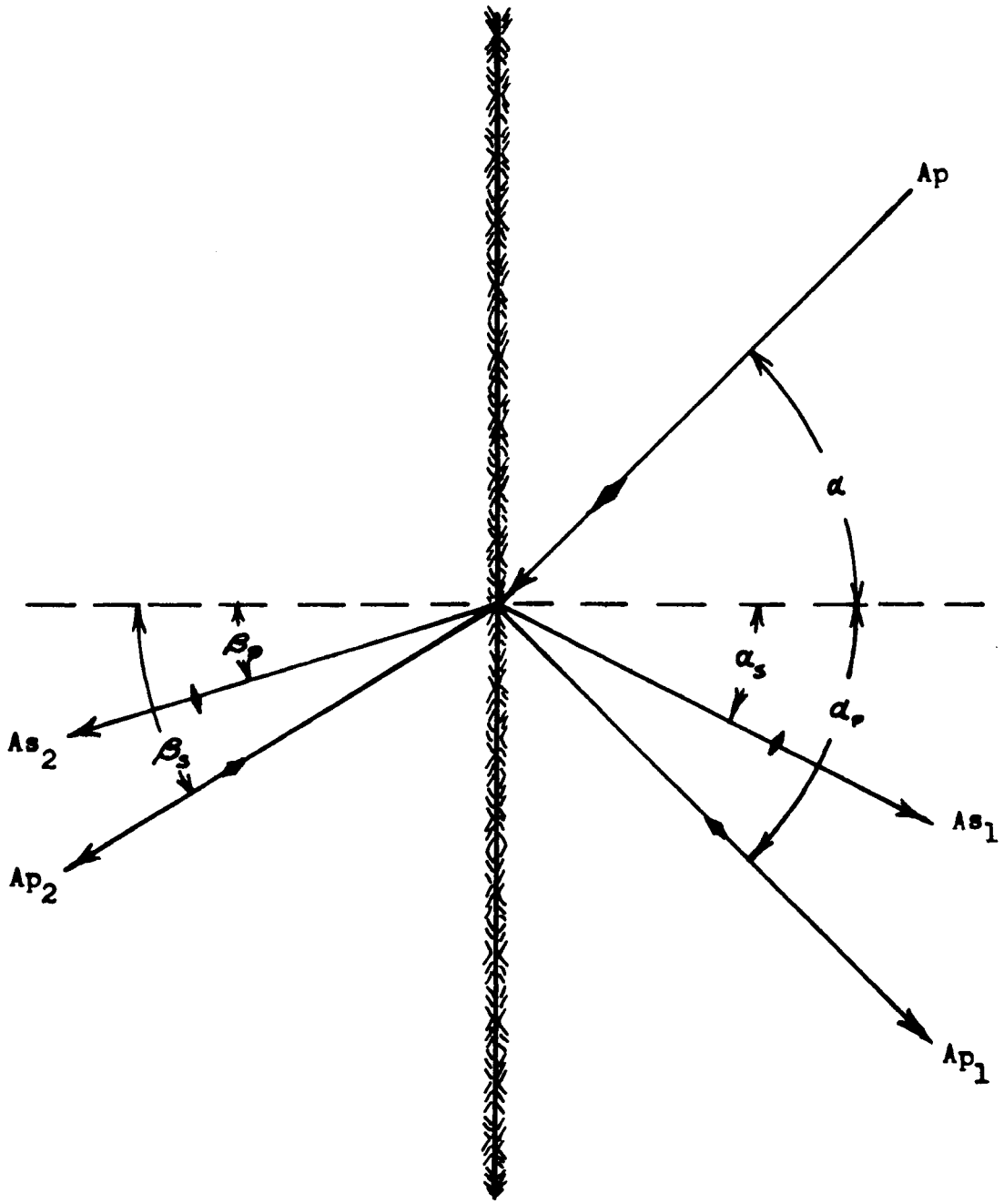

Figure 4. Partitioning of a P-Wave Stress When Striking an Impedance Discontinuity (Ref. 29, 31, 45, 57).

$$(A_p - A_{pl})\ (\sin 2\alpha)\ (V_s/V_p) = A_{sl}\left[1-2\sin^2\alpha\,(V_s/V_p)^2\right], \qquad (2)$$

$$\text{and } (A_p + A_{pl})\ \left[1 - 2\sin^2\alpha\,(V_s/V_p)^2\right] = A_{sl}\,(2\sin\alpha)\,(V_s/V_p)^2\ \left[1 - \sin^2\alpha\,(V_s/V_p)^2\right]^{0.5}. \qquad (3)$$

Solving the two equations simultaneously permits determination of the theoretical magnitudes of the reflected P and S stresses in terms of the initial compressive P-stress for specific values of α and μ. Figure 5 shows the plots of the relationships for several α and μ values.

It can be noted from the plots of the relative magnitudes for the reflected P and S stresses that for most real materials the generated shear (S) stress become increasingly important for the larger incident angles. For μ values less than 0.26, there also will be ranges of incident angles over which there would be no reflected P-stress (or tension). When the reflected shear stress becomes significantly larger in magnitude than the reflected tensile stress, shear failure rather than slabbing, or tensile rupturing, could well account for the bulk of fracture initiation.

The end-initiated cylindrical charge with a large L/D ratio presents additional complexities in regard to the respective influences of the shear and tensile rupture mechanisms. Referring to Figure 3, it can be seen that as the L/D ratio increases, more and more of the stresses in a wave front, if assumed to exhibit a conical wave form or shape, would strike at incident angles limited by the value of angle $\underline{c}$, where $\underline{c}$ is defined by the relationship $\sin \underline{c} = V_p/V_e$. Exceptions would be in the immediate region of the charge where initiation begins. Therefore, one

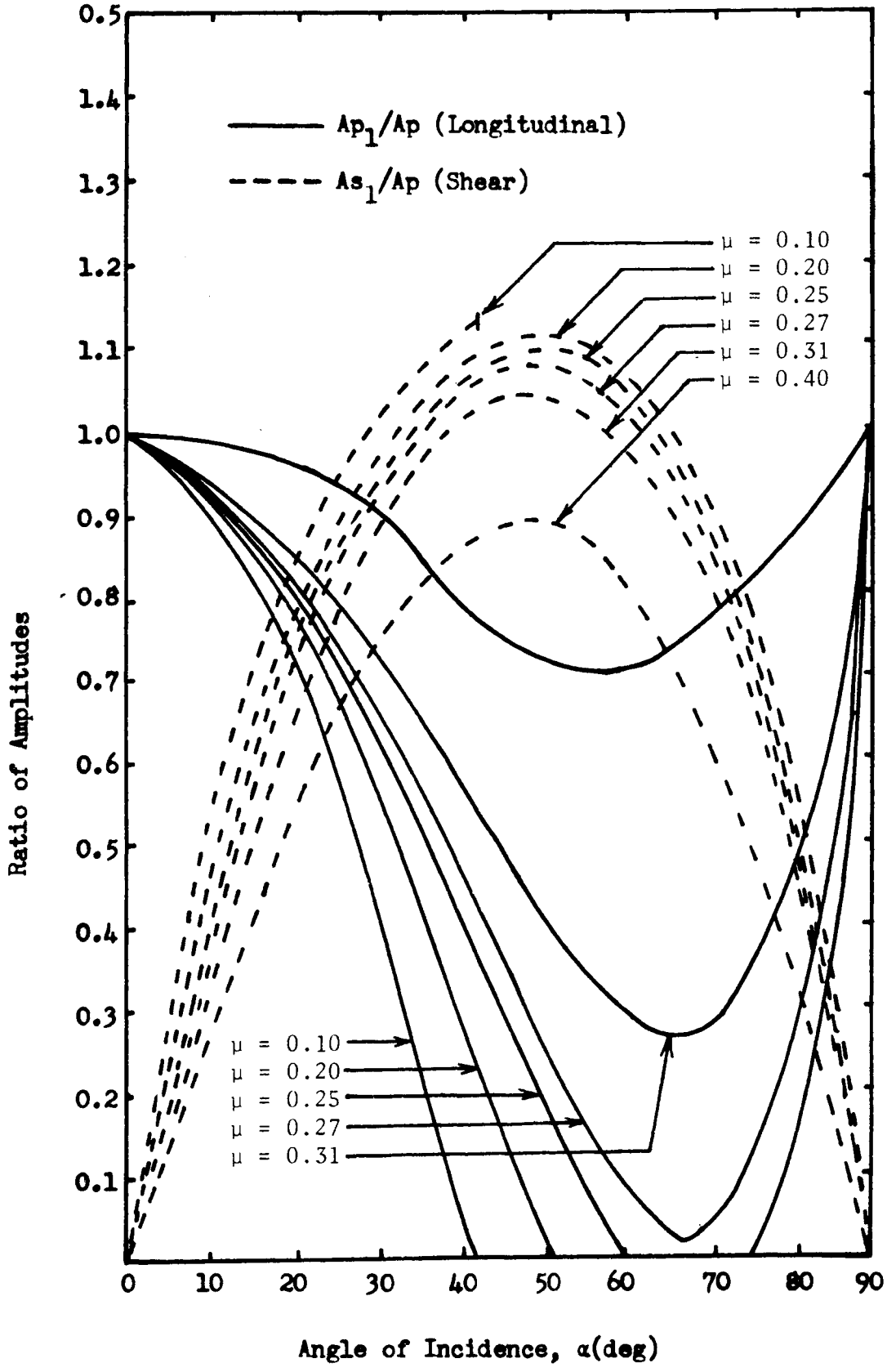

Figure 5. Relationships of Reflected Wave Amplitudes to that of an Incident P-Pulse at an Air Interface for Different Values of Poisson's Ratio (57).

could assume that for the majority of fracture initiation in the formation of craters by long cylindrical charges that only low magnitudes of reflected tensile (P) stresses would be formed. The significance of this conclusion is that for end-initiated long charges the extent of slabbing due to tensile stressing alone could be expected to be very limited, or absent completely in certain circumstances.

III. EXPERIMENTAL PROCEDURE

A. Model Preparation.

To study the influence of materials properties on cratering and fracturing mechanisms, specimens with widely varying characteristics were selected: Hydrostone, Plexiglas, mortar, and Jefferson City Dolomite, the latter being a very heterogeneous rock common to the local area. Most of the materials properties had been extensively tested by others (60, 61, 62, 63, and 64), so that only a minimum amount of measuring for essential data would be required. The Hydrostone and Plexiglas specimens were already available in appropriate forms for testing. The Hydrostone was in 6-inch cubes while the Plexiglas was in 4-inch cubes. The mortar required mixing and casting, and the dolomite needed only to be cut into the proper size. To simplify analyses of stress wave-forms, two model shapes for the mortar were selected: cubes and cylinders. Dolomite samples could be prepared in the size desired only in cubic form.

1. Selection of Explosive Charge-Length and Model Size.

In determining a suitable size for models, a limited series of initial tests was performed on available pre-cast mortar specimens. The pre-cast blocks were in 6-inch, 10-inch, and 12-inch cubes, respectively. Three-inch lengths of 10 and 20-grain Mild Detonating Fuse (MDF) and 50-grain plain Primacord detonating fuse were loaded and initiated in centrally drilled charge holes. Table 1 lists the properties of the detonating fuses used.

The smaller cubes, or 6-inch, appeared to be the most satisfactory

for use with both types of MDF. The 10-grain MDF, however, produced only fractures without separating the specimens. Therefore, it was decided to standardize on the 20-grain MDF to ensure that specimens split apart for easy observation.

Because it was desired to observe effects from charges with L/D ratio exceeding 10, a minimum charge length of 1.5 inches would be required. Thus, use of a standard 3-inch charge column would ensure a L/D ratio of 24 in the 6-inch models. In this latter case charge bottoms for centrally loaded specimens would be geometrically balanced with respect to all but the face at the hole collar.

Table 1.

Detonating Fuse Properties (65, 66).

Type	PETN core (gr/ft.)	Outside Diam. (in.)	V_e (fps)
MDF A-10	10	0.105	24,000
MDF A-20	20	0.123	22,000
Plain Primacord	50	0.198	21,000

2. Mixing, Casting, and Cutting of Specimens.

Batches of mortar were prepared using 4 parts of washed, small grain, locally available commercial river-sand, 2 parts of Portland cement, and 1 part water, all proportions being by weight. Small quantities of each ingredient were alternately loaded into a power driven, rotary, paddle-type mixer. A full batch was then mixed for 45 minutes. Following mixing, each batch was poured into pre-fabricated

appropriately shaped molds. To ensure the elimination of air bubbles, care was taken to vibrate and tamp the unconsolidated mortar with the aid of two 1/2-inch diameter steel rods. Specimens were then allowed to set for 24 hours, after which they were removed from the molds and cured at 40 degrees Fahrenheit and 100% relative humidity for 8 days.

The cubic molds were made of 0.5-inch plywood. The rim and groove type of mold, held together by two end bolts, permitted casting of three samples at the same time (Plate I). Cylinders were cast in heavy cardboard, paraffin coated, containers with one end covered by a metal disk.

The pre-cast Hydrostone specimens were made of 4 parts U.S. Gypsum Hydrostone and 1 part water, both proportions by weight. Mixing was done by hand in an 18-inch diameter by 7-inch high container, which allowed only 22-lb. batches, or enough for 3 models. Setting time before removal from molds was one hour, while curing out of the molds consisted of 30 days.

Models of Plexiglas prepared earlier had been cut from a 4 x 24 x 48-inch sheet of stock manufactured by The Rohm & Haas Company. Cutting into 4-inch cubes was accomplished by means of a wood table saw.

After securing reasonably solid slabs of Jefferson City Dolomite from the UMR Experimental Mine property, appropriate 6-inch cubes were cut by means of a Model U, Highland Park, 24-inch x 0.105-diamond rock cutting saw. Since kerosene was used as the coolant and lubricant during the cutting, samples appeared to contain a small amount of kerosene near the model surfaces. However, this condition was not considered to adversely affect the results.

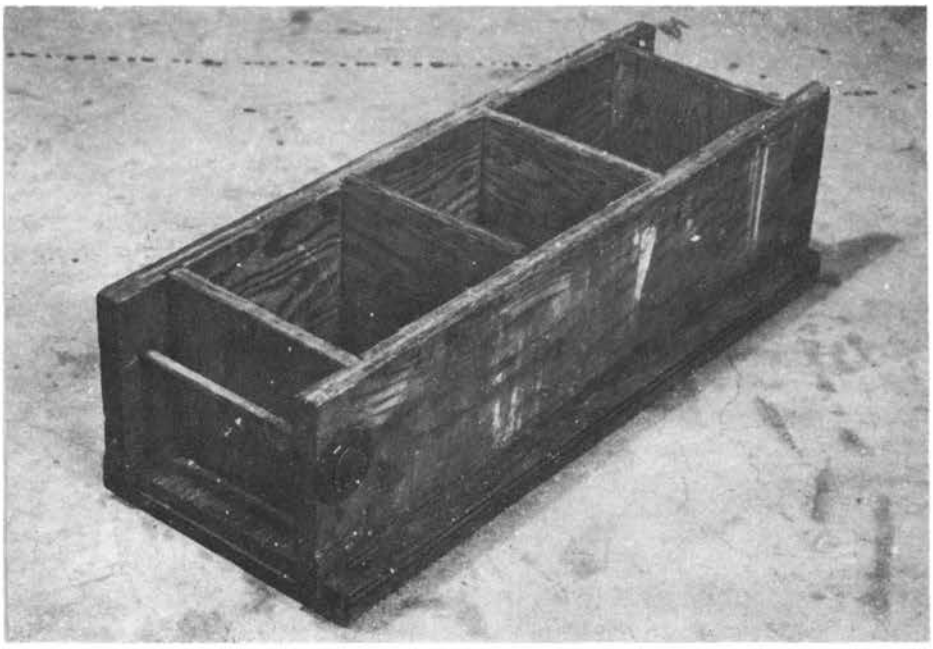

Plate I. Rim and Groove Type of Mold for Cubes of Mortar.

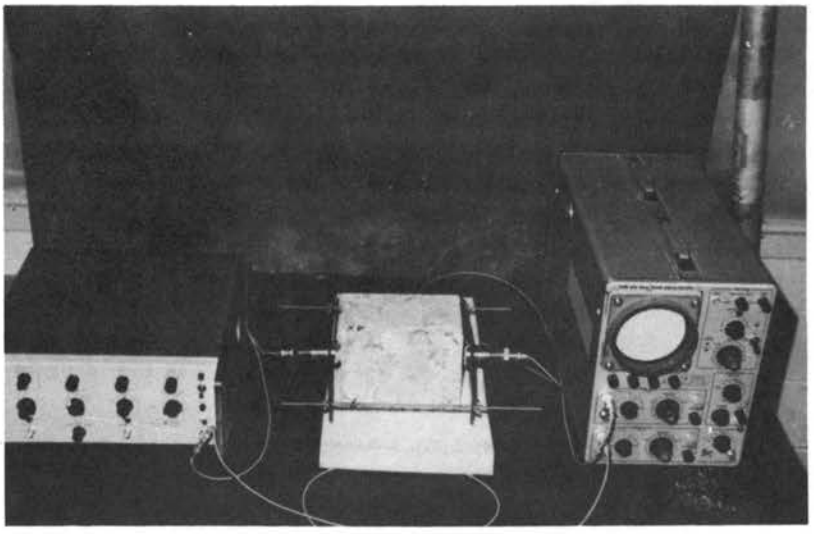

Plate II. Instrumentation for Longitudinal Wave Velocity Measurements.

3. Soaking of Models.

Approximately half the number of specimens available of each material, excluding Plexiglas, were soaked in water-filled containers until no further significant gain in weight was realized. Dolomite and mortar specimens took about 15 days to attain this condition, while Hydrostone took only 3 days.

B. Determination of Physical Properties.

Table 2, is a summation of average materials' properties pertinent to this investigation. Where it was felt properties could not be approximated accurately, particularly for models mixed in the laboratory, measurements were made to obtain data. Properties of materials used as refractive media at interfaces were obtained from various sources.

1. Density.

Each model sample was weighed and measured to the nearest gram and 1/16-inch, respectively, from which the density (d_m) was computed. A check was made by determining the specific gravity of small samples of each material. A small fragment was weighed, and its volume measured from the volume of water displaced in a graduated cylinder (Appendix II).

2. Longitudinal Wave Velocity.

The characteristic longitudinal wave velocities of selected dry and wet specimens were determined by the sonic pulse method. The instrumentation (Plate II) was designed by J. H. Deatherage[67], a complete description of which is included in his M.S. Thesis. The

Table 2

Materials' Properties (67, 68, 69, 70, 71, 72)

Material	V_p (fps)	$\underline{c}$ (deg)	d_m (pcf)	z (ps/cf)	μ	σ_c (psi)	σ_t (psi)	τ_s (psi)	τ_s/σ_t
Plexiglas	9,000	24	74	21,400	0.40	11,000	7,500	11,000	1.5
Hydrostone, dry	11,000	30	106	36,600	0.18	7,200	2,000	6,000	3.0
wet	10,200	28	110	35,000	----	-----	-----	-----	----
Mortar, dry	13,200	37	138	56,700	0.20	4,000	400	2,600	6.5
wet	13,300	37°30'	140	58,000	----	-----	-----	-----	----
Dolomite, dry	14,800	42	156	71,700	0.27	9,000	220	7,500	34.1
wet	12,200	34	160	61,000	----	-----	-----	-----	----
Air	1,100	--	0.076	2.6	-----	-----	-----	-----	----
Water	4,750	--	62.4	9,200	0.50	-----	-----	-----	----
Concrete	13,200	--	138	56,700	0.20	-----	-----	-----	----
Steel	20,000	--	490	304,000	0.31	-----	-----	-----	----

technique utilized crystals of lead-zirconate titanate, placed at opposite ends of specimens.

An electric pulse generated by a pulse generator was applied to one of the crystals. The crystal transformed the electrical pulse into a mechanical pulse, in turn, which traveled through the material as a longitudinal wave. The disturbance was sensed by the other crystal, which transformed the mechanical pulse back into an electrical one. This latter pulse was fed into an oscilloscope, along with a synchronizing pulse, from which the time required for pulse travel through a measured length of specimen could be recorded to the nearest half microsecond. Knowing the length of each specimen, the longitudinal wave velocity could be easily calculated (Appendix III).

3. Accoustical Impedance, Poisson's Ratio, and Ultimate Strengths.

From the density, d_m, and the longitudinal velocity, V_p, the characteristic impedance, z, of each material was calculated, where $z = \rho_l V_p$, in which ρ_l is the mass density and equals d_m/g. Thus, $z = d_m V_p/g$. The average impedance values for specimen and refractive materials shown in Table 2 were determined in this manner.

Approximate values for Poisson's ratio and the materials strengths were obtained from pertinent literature. Since the nature of this investigation was not quantitative and exact stress values were not required, it was felt that reasonable approximations could be made under the circumstances. The purpose of including these properties was to provide a relative basis upon which to analyze probable causes for fracture and crater development in specimens, as a function of

changing incident angles for the stress pulses.

C. Placement and Firing of Charges.

Drilling of charge holes was accomplished by means of tungsten-carbide tipped, straight shank, taper length, Type 1120, Chicago-Latrobe drills, operated in a drill press (Plate III). A 1/8-inch diameter drill was used for the 10-grain MDF and a 9/64-inch size for the 20-grain MDF. Plexiglas and Hydrostone could be drilled with no difficulty, but the mortar and dolomite required withdrawal of the drill after every 1/16 to 1/8-inch advance so cuttings could be removed by short blasts of compressed air. Attempts to drill granite were unsuccessful.

About 4-inches of MDF was necessary for each test, initiation being done externally for the 3-inch blast hole depths. An Atlas No. 6 electric blasting cap was taped to the protruding end of the MDF, with a shield plate placed between the initiator and the sample to eliminate effects of the cap. The shield was made of a 1/4 x 10 x 10-inch steel plate with a 9/64-inch hole drilled in the center to permit passage of the MDF (Plate IV). The test specimens were then enclosed within a blasting chamber, constructed of steel and lined with 3 inches of wood. A 45-volt radio B-battery was used as the power source.

Photographs were taken of each specimen after firing, so that a permanent visual record would be available of test information. In addition, angles a and b and the average fragment thickness, s, if present, were measured and recorded (Appendix IV).

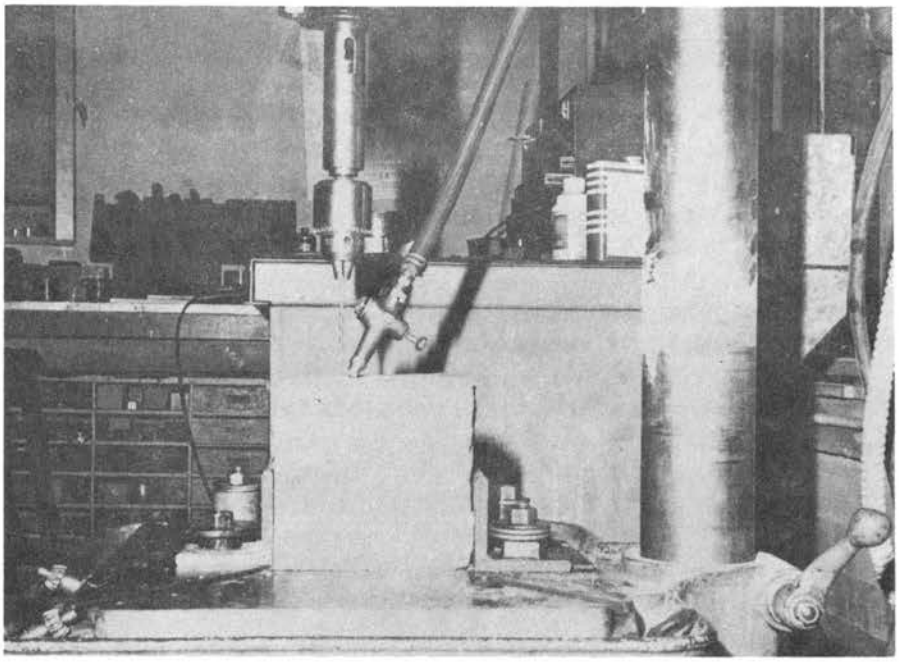

Plate III. Arrangement for Drilling Charge Holes.

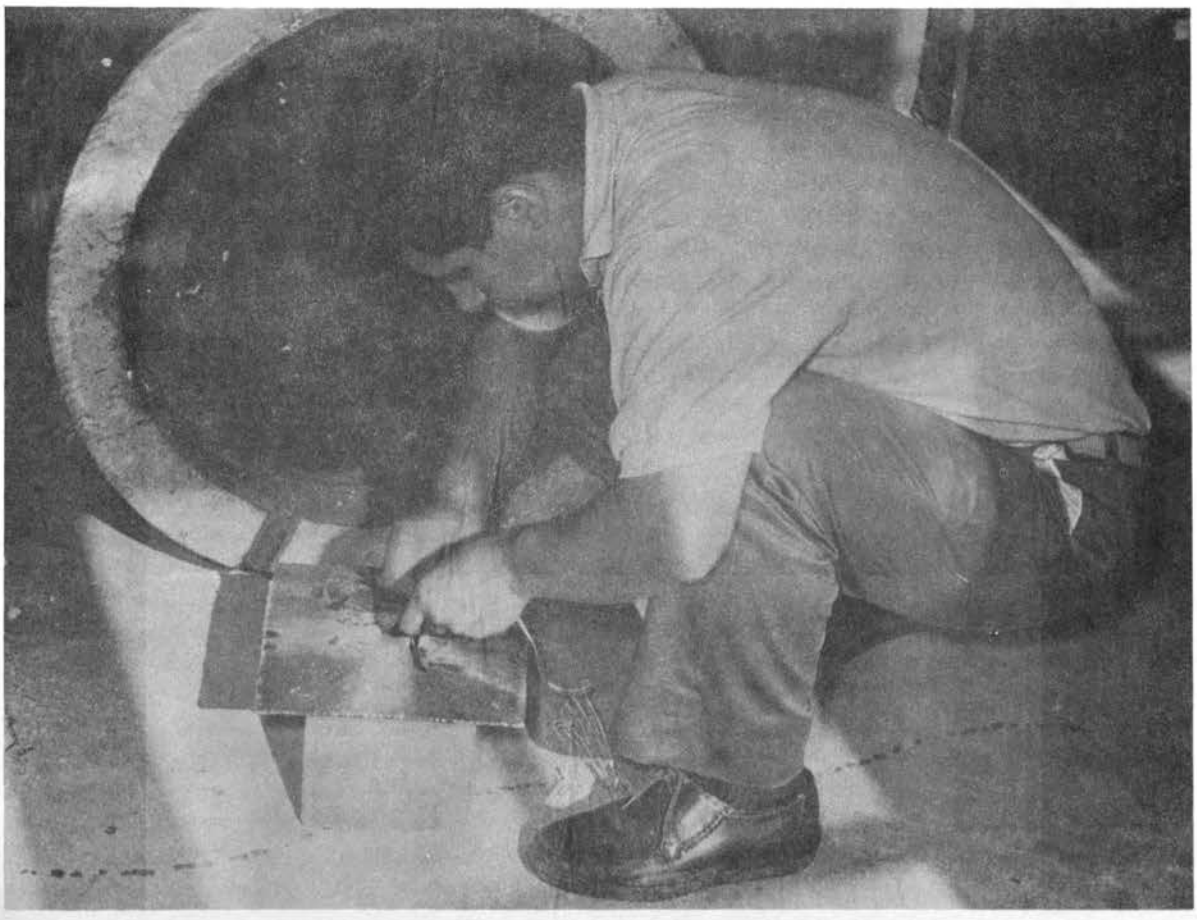

Plate IV. Preparing a Charge for Firing.

IV. DISCUSSION OF RESULTS

To evaluate blast effects from charges for the various blasting environments, in addition to visual evidence recorded on photographs, three specific crater parameters were analyzed. The latter included (a) fragment shape and thickness, s, measured in the charge diameter plane along the burden dimension, (b) the top horizontal free-face angle, a, of the crater outline developed in the plane of the charge diameter and (c) the front vertical free-face angle, b, of the crater outline developed in the plane of the charge length, L (Fig. 2).

As discussed earlier in Chapter II, the conical wave-form generated by the MDF cylindrical charges should have produced stress waves most of which propagated along a common angle c with the charge length (Fig. 3). Angle c would have been defined by the inverse of the velocity ratio, i.e., $\sin c = V_p/V_e$, characteristic of the particular specimen used and the MDF. Since the velocity of the MDF was constant for all tests, any variation in the value of c should have been due only to the longitudinal velocity distinctive of the specimen studied (see Table 2 for specific data). The significance of the value of angle c is that it should control the smallest angle of incidence, α, at which most of the stresses along the wave front would strike the free face paralleling the explosive charge length. Except in the vicinity of the end at which a charge was initiated the angles of incidence for stresses in each vertical plane passing through the charge should remain constant along a major portion of the vertical free face, if a conical wave form had been generated by the long

charge. The constancy of angle c would be independent of the accoustical impedance relationship between the media at the interface boundary and of the burden.

If a conical wave was propagated by the end-initiated cylindrical charge, the shape of fragments formed quite likely could be strongly influenced by angle c. On the other hand, the fragment thickness, s, would be a function of the compressive wave amplitude propagated by the charge, the accoustical match of the two media bounding an interface, and the stress incidence angles, α , the lowest value of which would be angle c. As the burden dimension increased, the thickness should decrease since the stress amplitudes would decrease with distance. On the other hand, as impedance differences at interfaces increased, the thickness should increase. This is because more of the initial compressive pulse would be reflected.

Results from these tests evidenced clearly that a conical wave was propagated by the end-initiated cylindrical charge. Tests conducted initially in Plexiglas showed definite conical fracture patterns within specimens (Plates V and VI). Additional evidence of the conical wave-form generated was shown by the production of cones, humps, or plugs, depending on test conditions (Plates V, VII through XV). Fragments in practically all cases tended to be in the shape of wedges that tapered downwards, or in the direction of reaction travel through the explosive column (Plates VII, VIII, XII, XV, and XVI). The fragment thicknesses decreased with larger values of angle c, as expected (Fig. 6 and 7), while thicknesses increased as impedance differences at interfaces became greater (Fig. 8).

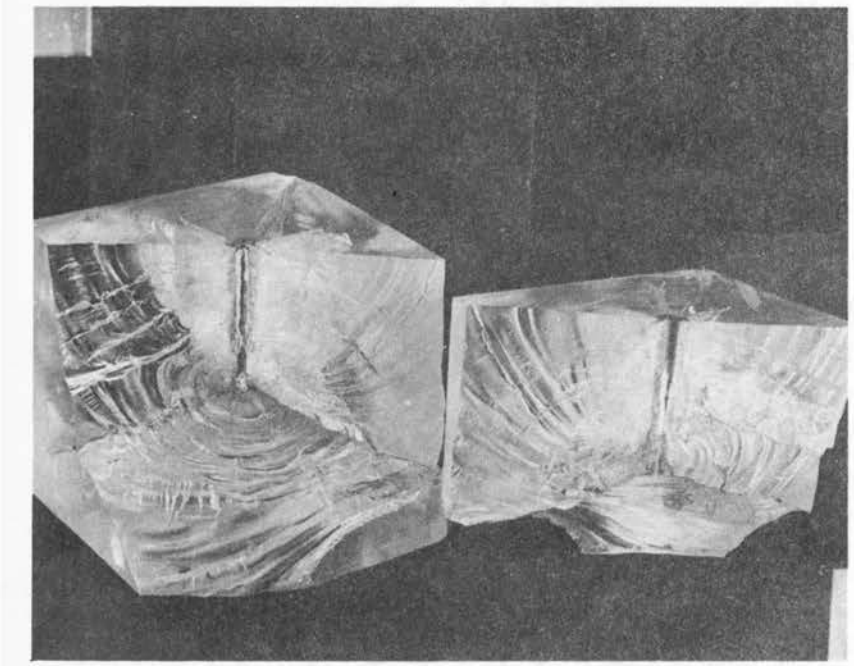

Plate V. Plexiglas Model Fired with 2-inch Deep Central Hole and 20 MDF.

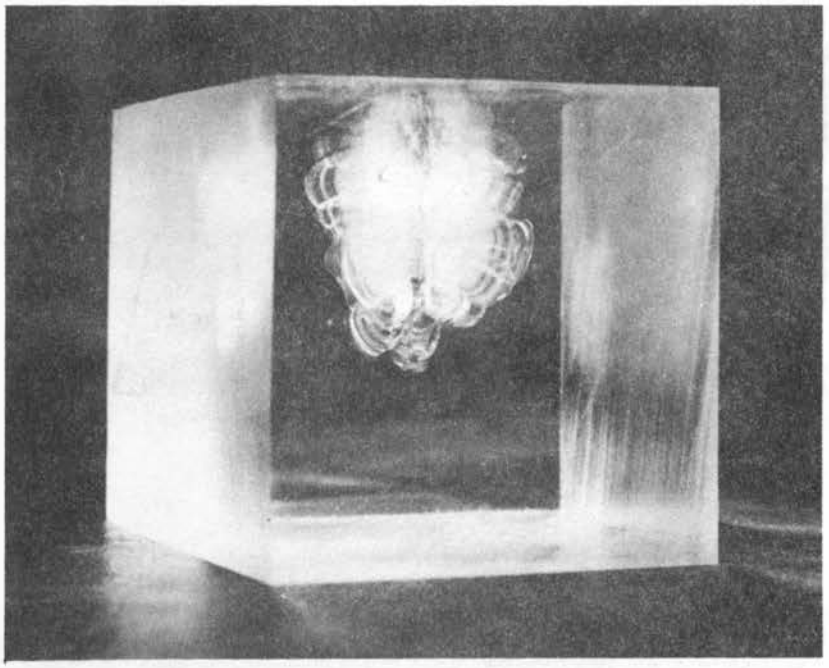

Plate VI. Plexiglas Model Fired with 10 MDF.

Plate VII. Dry Cylinder of Mortar Fired with 2-inch Burden and Bottom Face Placed on Concrete Surface.

Plate VIII. Wet Cylinder of Mortar Fired with 2-inch Burden and the Bottom Face Placed on Concrete Surface.

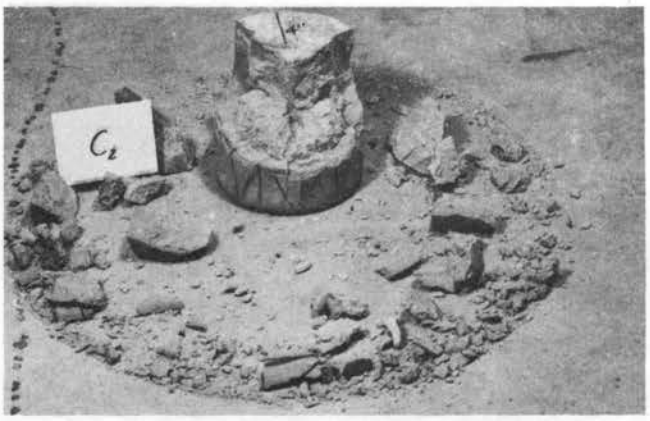

Plate IX. Wet Cylinder of Mortar Fired with 2-inch Burden and Air Interfaces.

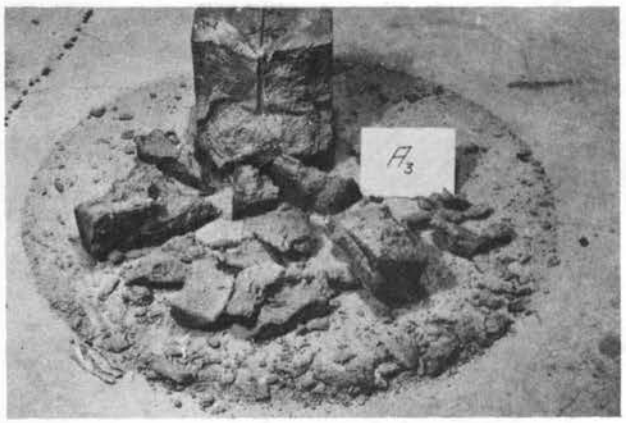

Plate X. Wet Cube of Mortar Fired with 2-inch Burden and Bottom Face Placed on Concrete Surface.

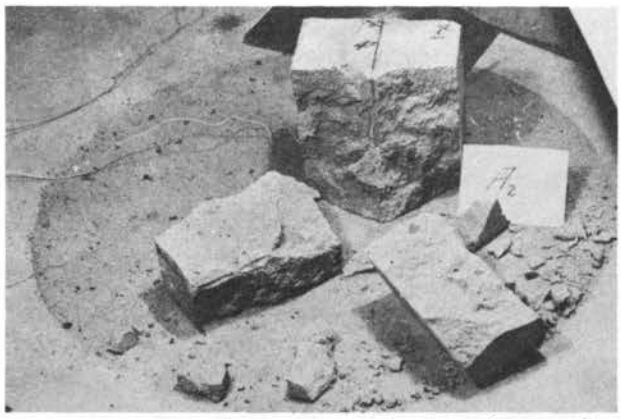

Plate XI. Dry Cube of Mortar Fired with 2-inch Burden and Bottom Face Placed on Concrete Surface.

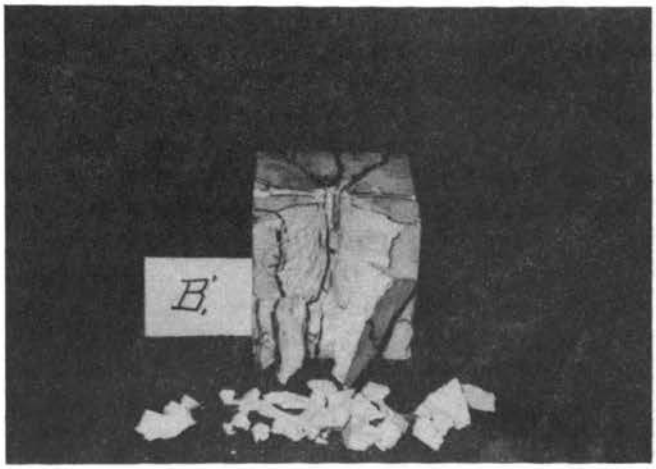

Plate XII. Dry Hydrostone Fired with 2-inch Burden and Air Interfaces.

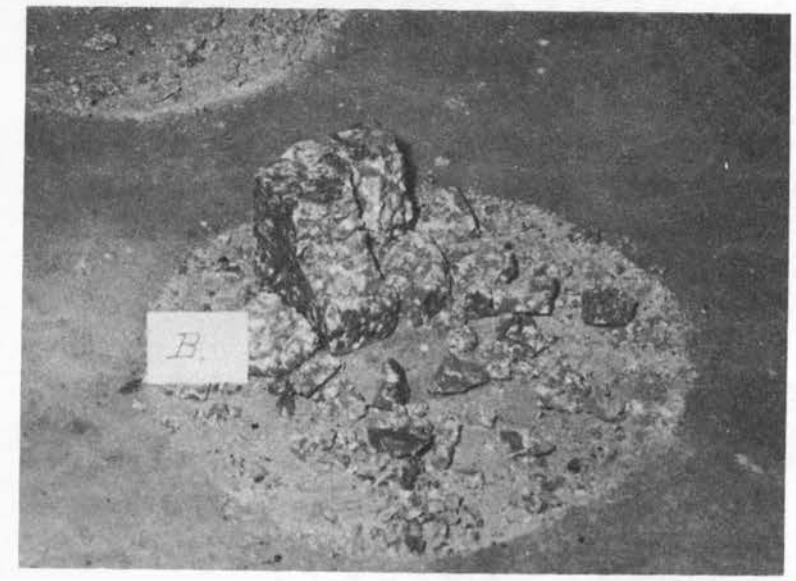

Plate XIII. Dry Dolomite Fired with 2-inch Burden and Bottom Face Placed on a Concrete Surface.

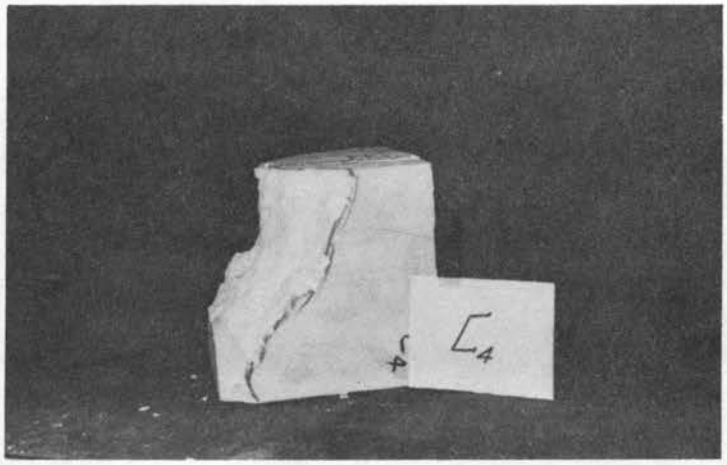

a. Side View.

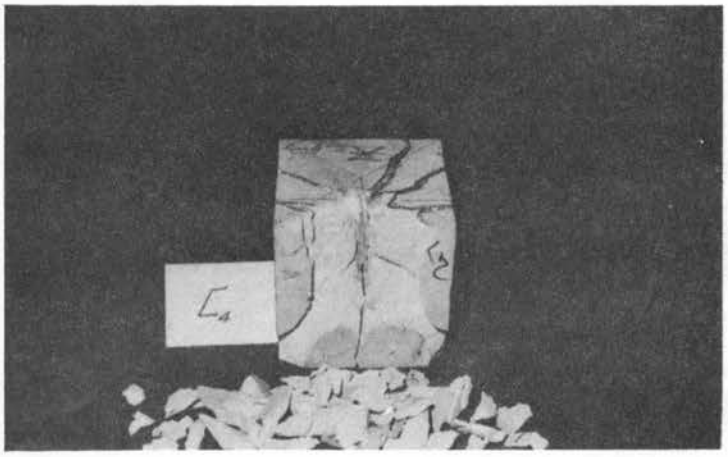

b. Front View.

Plate XIV. Dry Hydrostone Fired with 1.5 inch Burden and Bottom Face Placed on Concrete Surface.

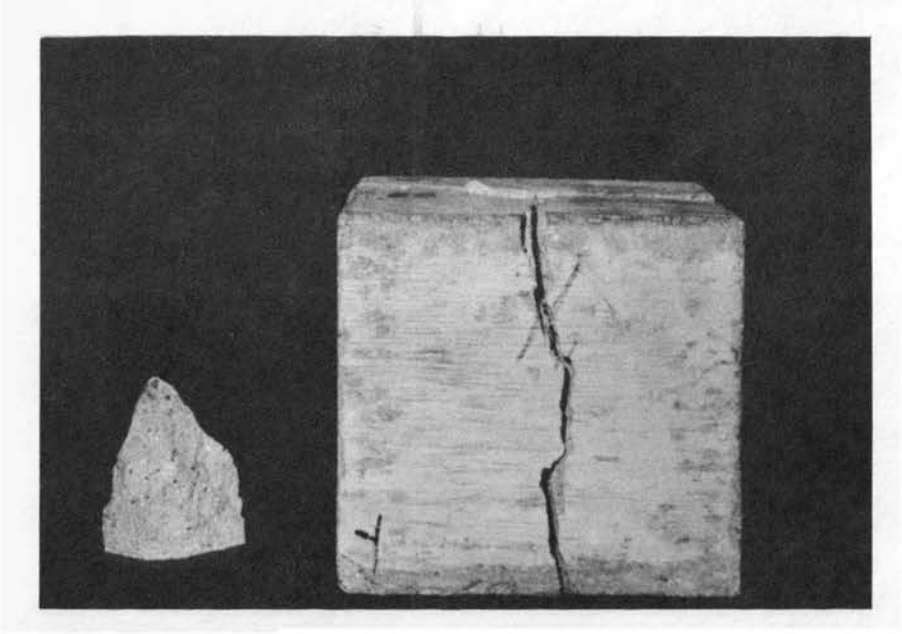

a. Side View

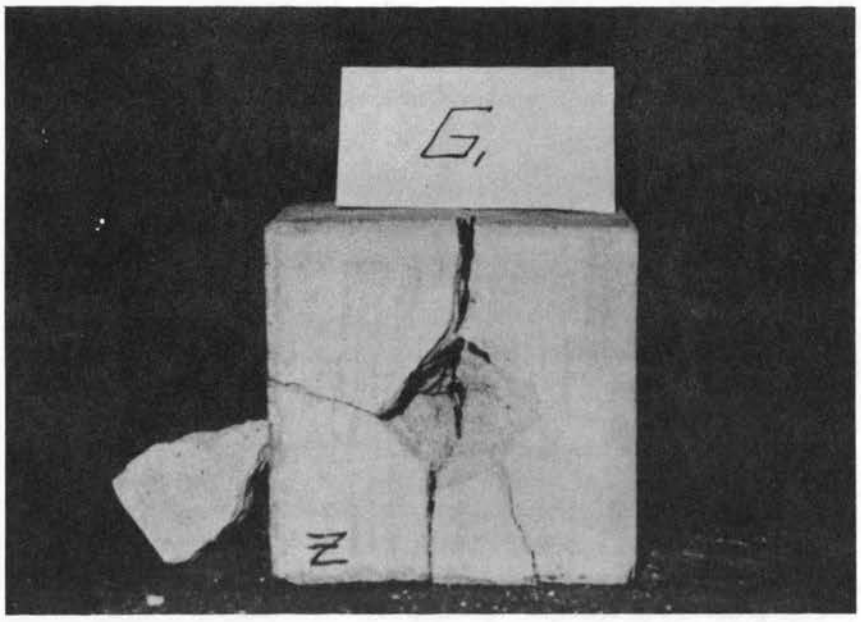

b. Bottom View

Plate XV. Dry Mortar Fired with 3-inch Burden and Air Interfaces.

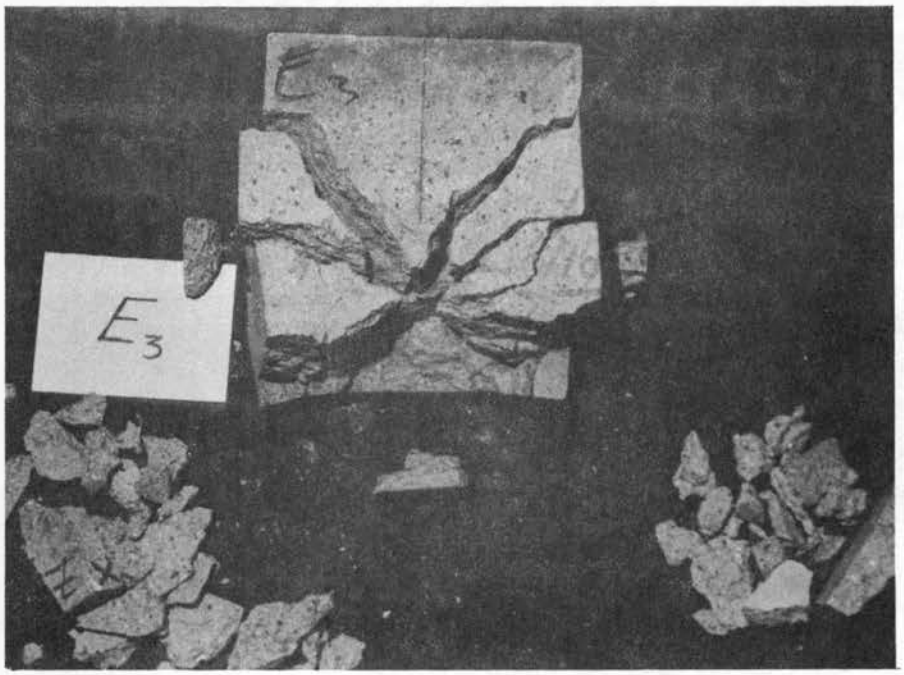

a. Top View.

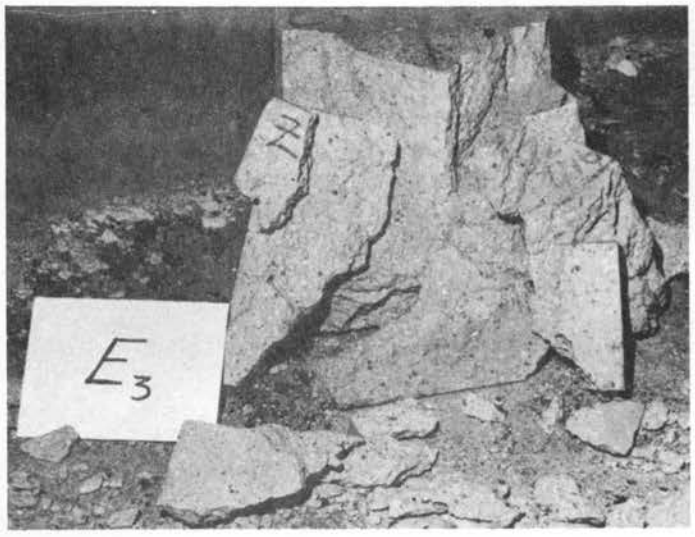

b. Front View.

Plate XVI. Wet Mortar Fired with 1.5-inch Burden and Bottom Faces Placed on a Concrete Surface.

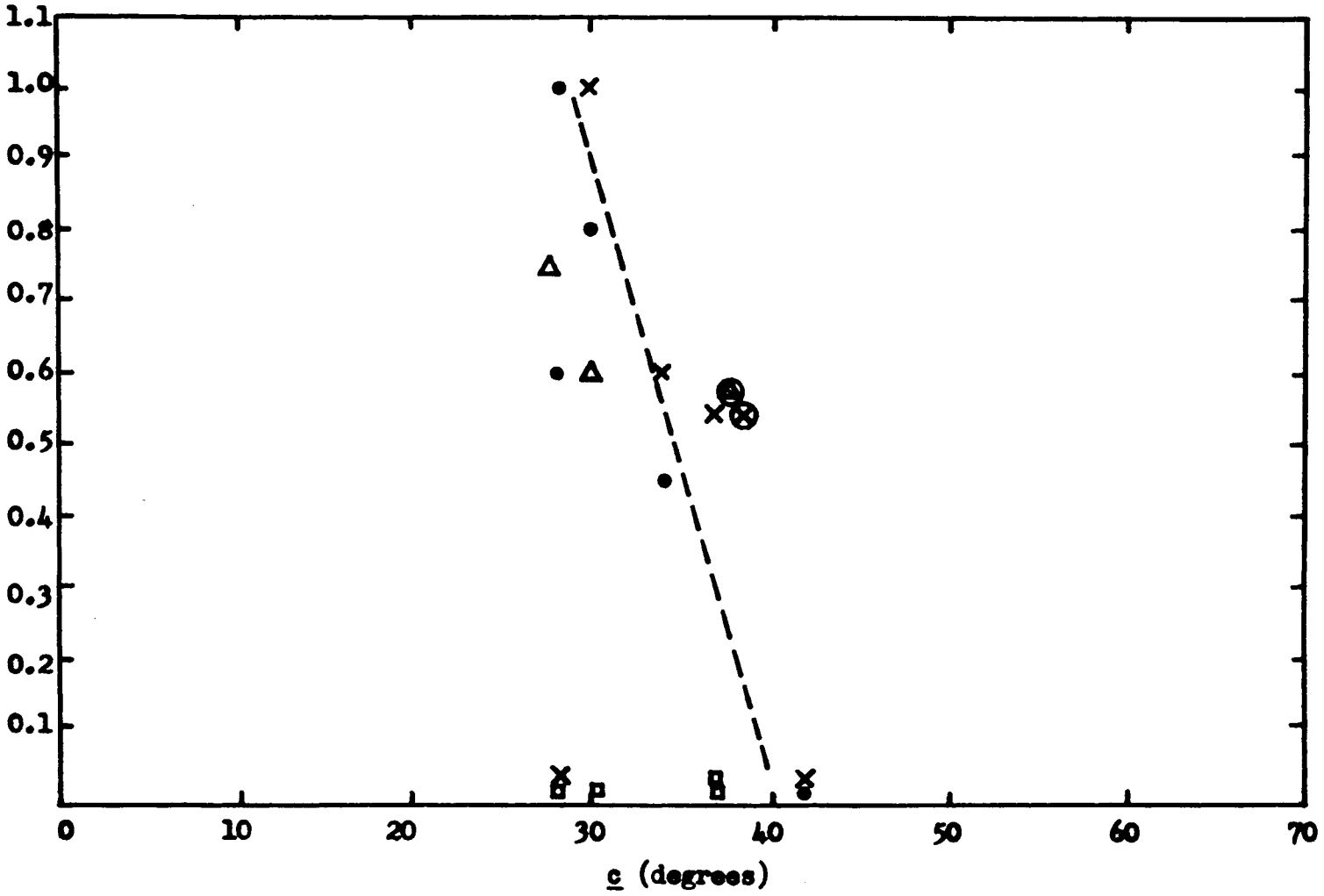

Figure 6. Stress Cone Angle vs. Fragment Thickness for Specimens with 2-inch Burden. (Note: See Appendix I, page 63, for symbols used in graphs.)

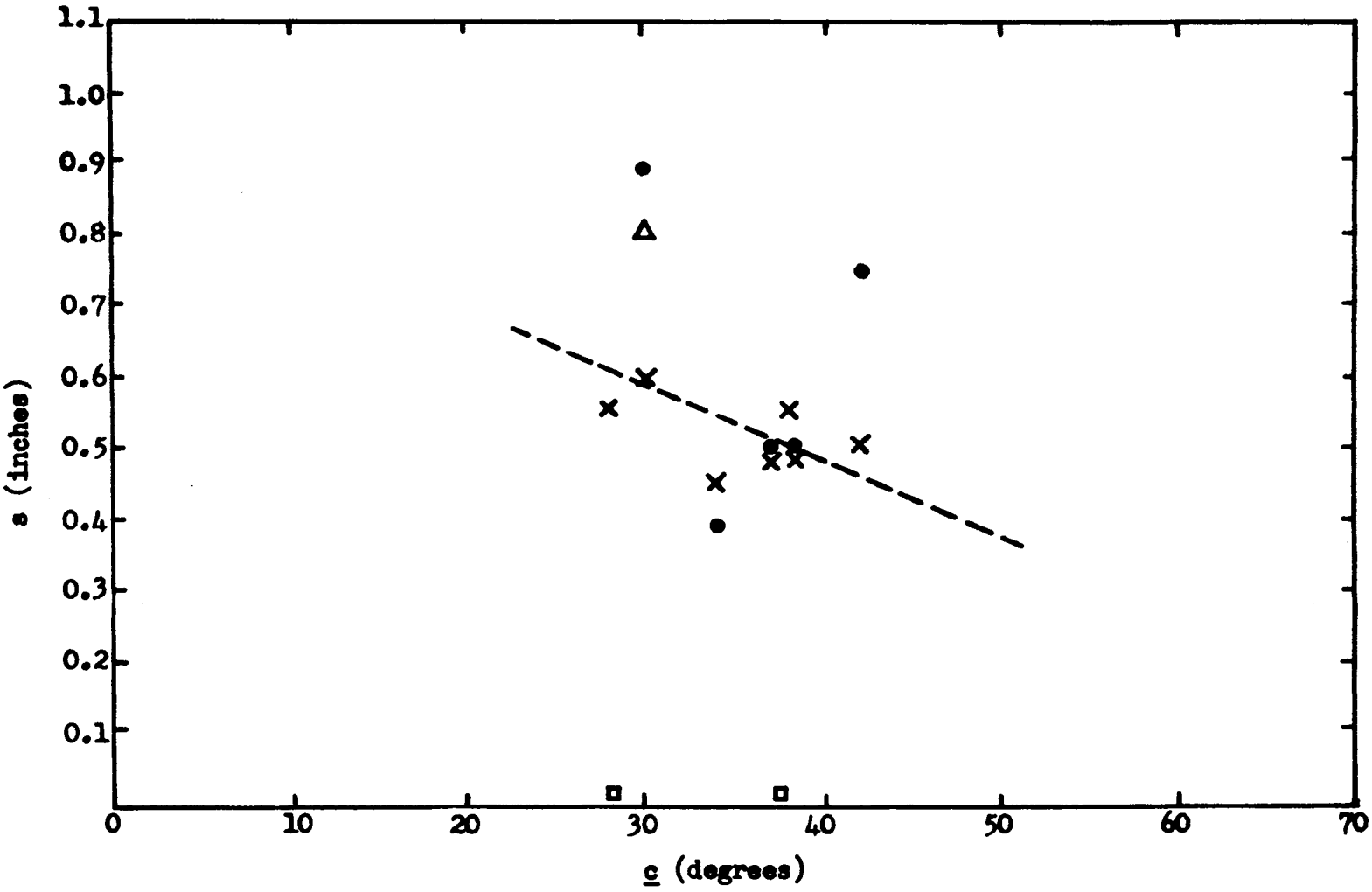

Figure 7. Stress Cone Angle vs. Fragment Thickness for Specimens with 1.5-inch Burden.

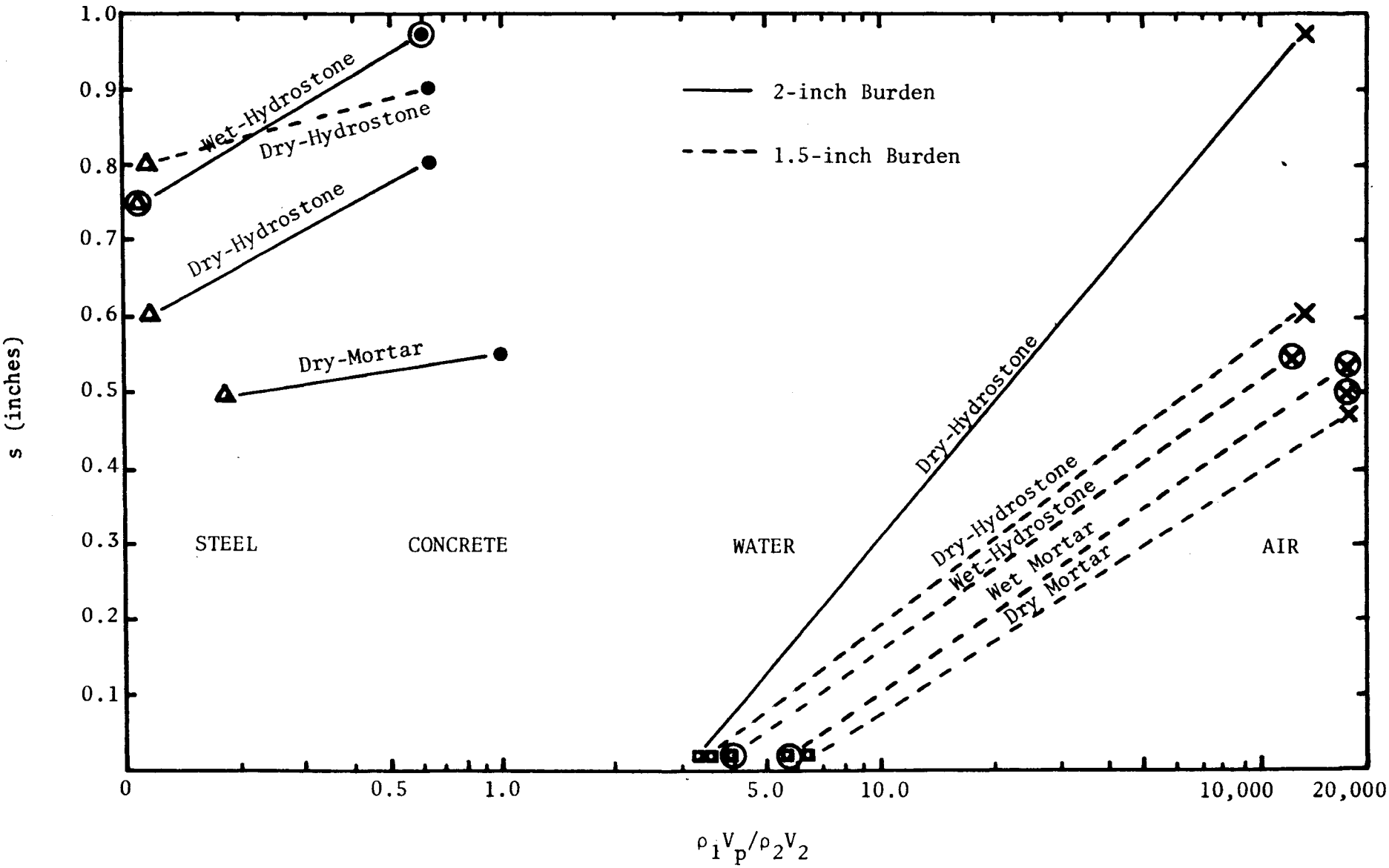

Figure 8. Impedance Differences at Free-Faces vs. Fragment Thickness for Specimens with 2 and 1.5-inch Burdens.

Angle a in the plane perpendicular to the charge length was considered an important crater parameter that could well be common to all confined explosive charges, i.e., cylindrical and spherical. However, it was desirable to investigate whether or not the conical wave-form generated by the end-initiated long cylindrical charge exerted any specific influence on its value. In addition, the effects of moisture content, material's properties, and geometric dimensions were of particular interest, as far as determining in what specific ways they might alter the theoretically assumed value for a of 45 degrees.

The conical stress wave propagated in a circular fashion in the plane of angle a as expected, evidenced by the uniformity of fracture patterns in that plane. Plates XVII, XVIII, and XIX, all show the effect clearly for centrally-loaded charges in cubic and cylindrical specimens of mortar, i.e., 3-inch burden. A symmetrical cratering process was also present for side craters, produced by 1.5 and 2-inch burdens (Plates IX, X, XII, and XIV). It should be noted, however, that the values of angle a were higher for cylindrical specimens than they were for cubic models, except for central loading where geometric balance was present (Fig. 9 and 10).

As a general rule, the value of angle a decreased as the burden, B, increased (Fig. 9, 10, 11, and 12). This was expected since the magnitude of the stresses normally should be reduced with distance. At similar burdens, the Hydrostone tended to crater at slightly larger angles than did the dolomite and mortar. There were very little differences in the values of angle a between the dry and wet specimens of the same material at the 1 1/2-inch burdens, but at the larger

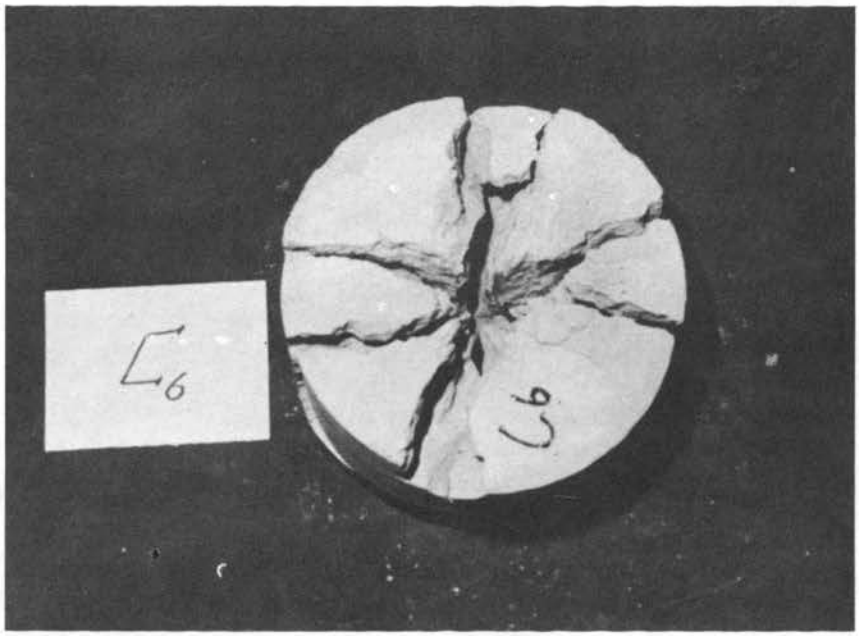

Plate XVII. Dry Cylinder of Mortar Fired with 3-inch Burden and Air Interfaces.

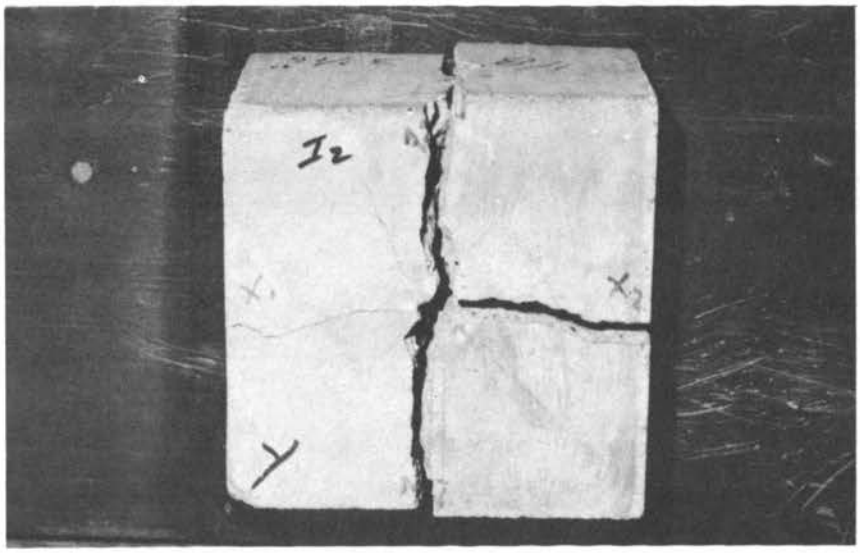

Plate XVIII. Dry Cube of Mortar Fired with 3-inch Burden and Air Interfaces.

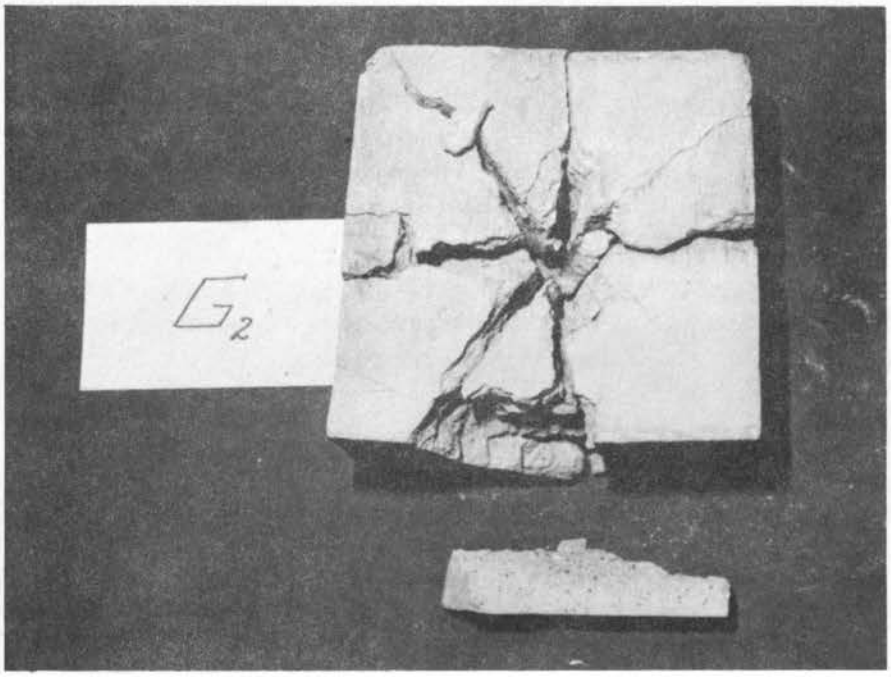

Plate XIX. Wet Cube of Mortar Fired with 3-inch Burden and Bottom Face Placed on a Concrete Surface.

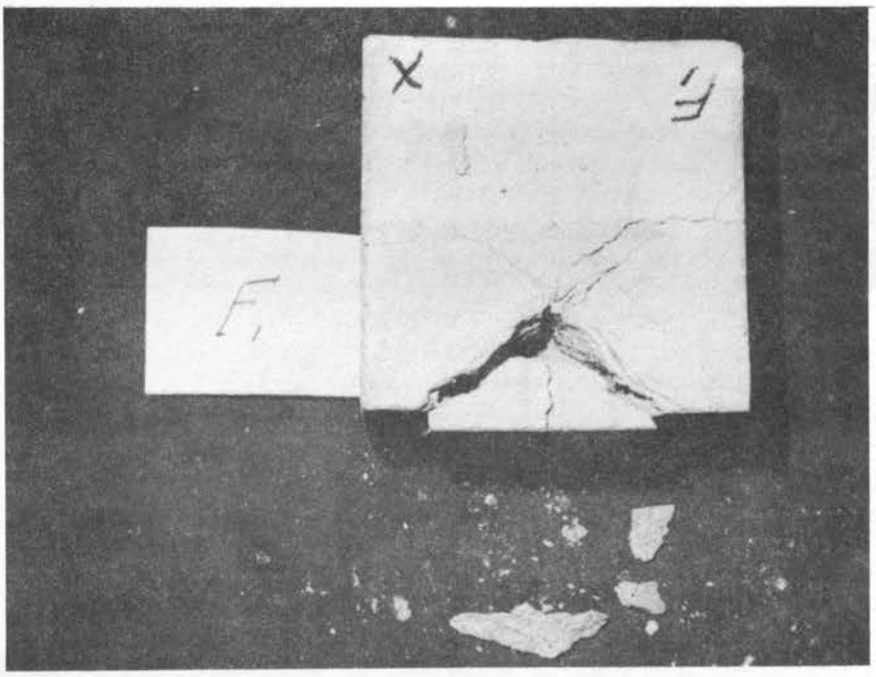

Plate XX. Dry Cube of Mortar Fired with 1.5-inch Burden and Water Interfaces.

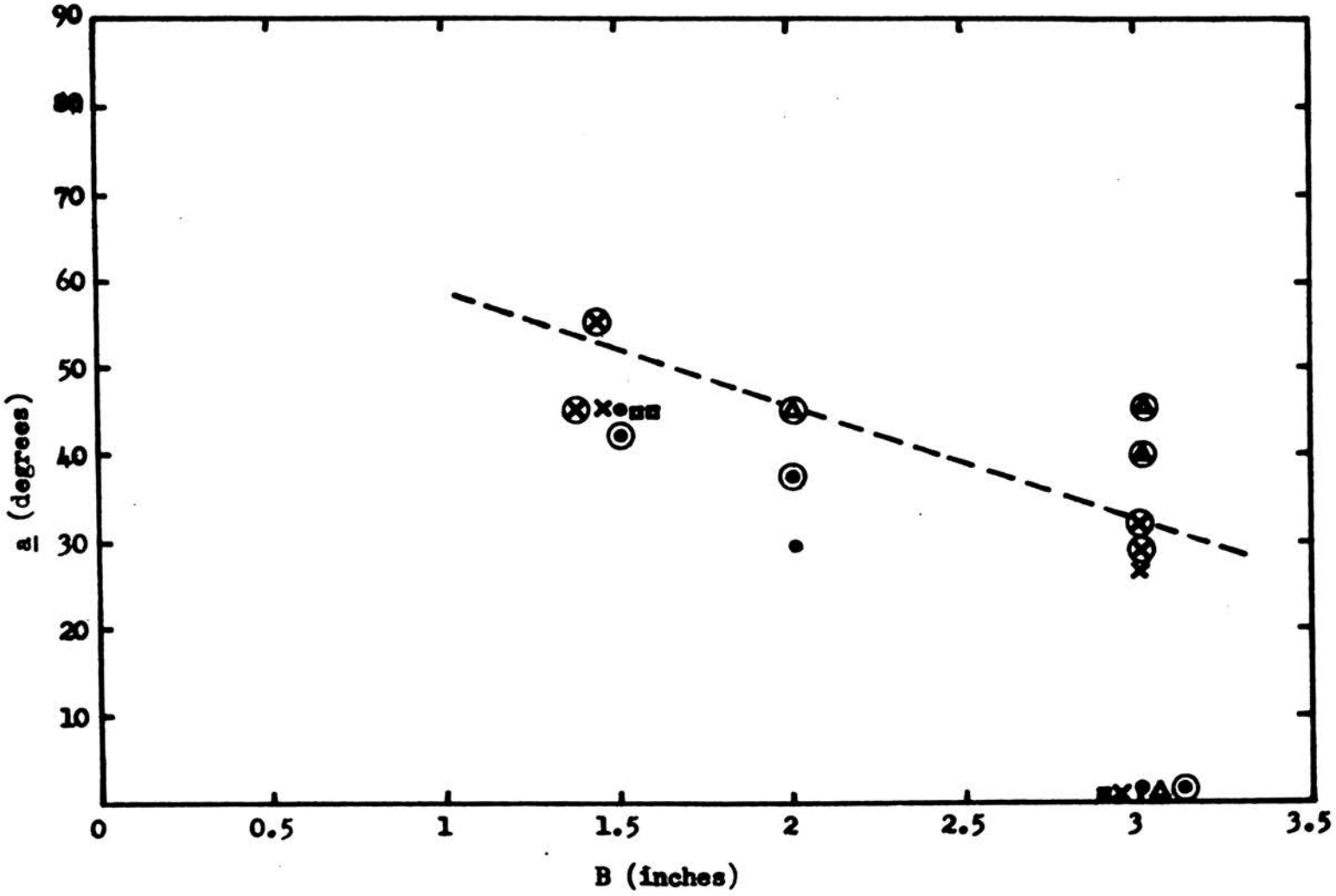

Figure 9. Burden vs. Crater Angle a for Cubes of Mortar.

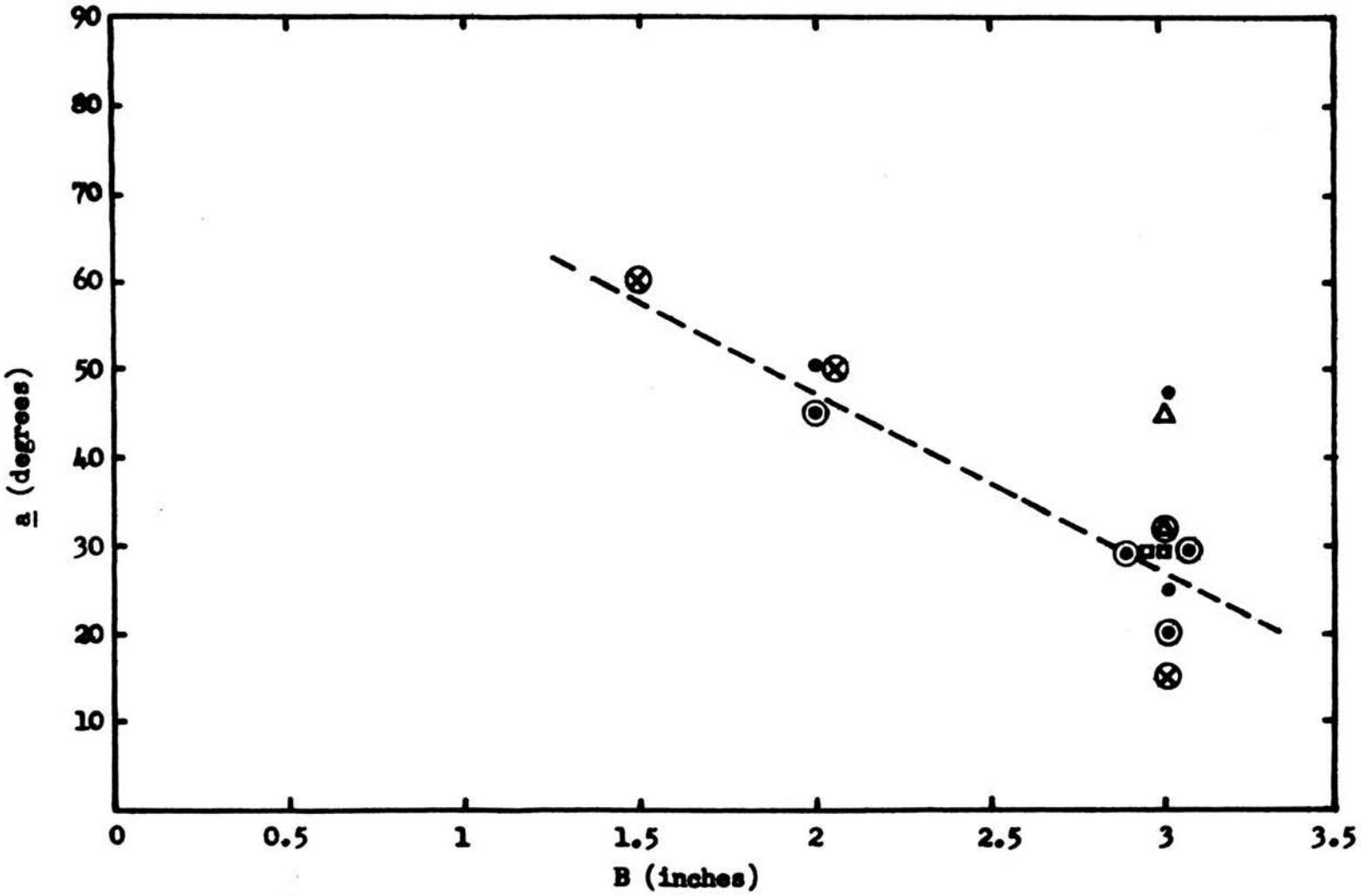

Figure 10. Burden vs. Crater Angle a for Cylinders of Mortar.

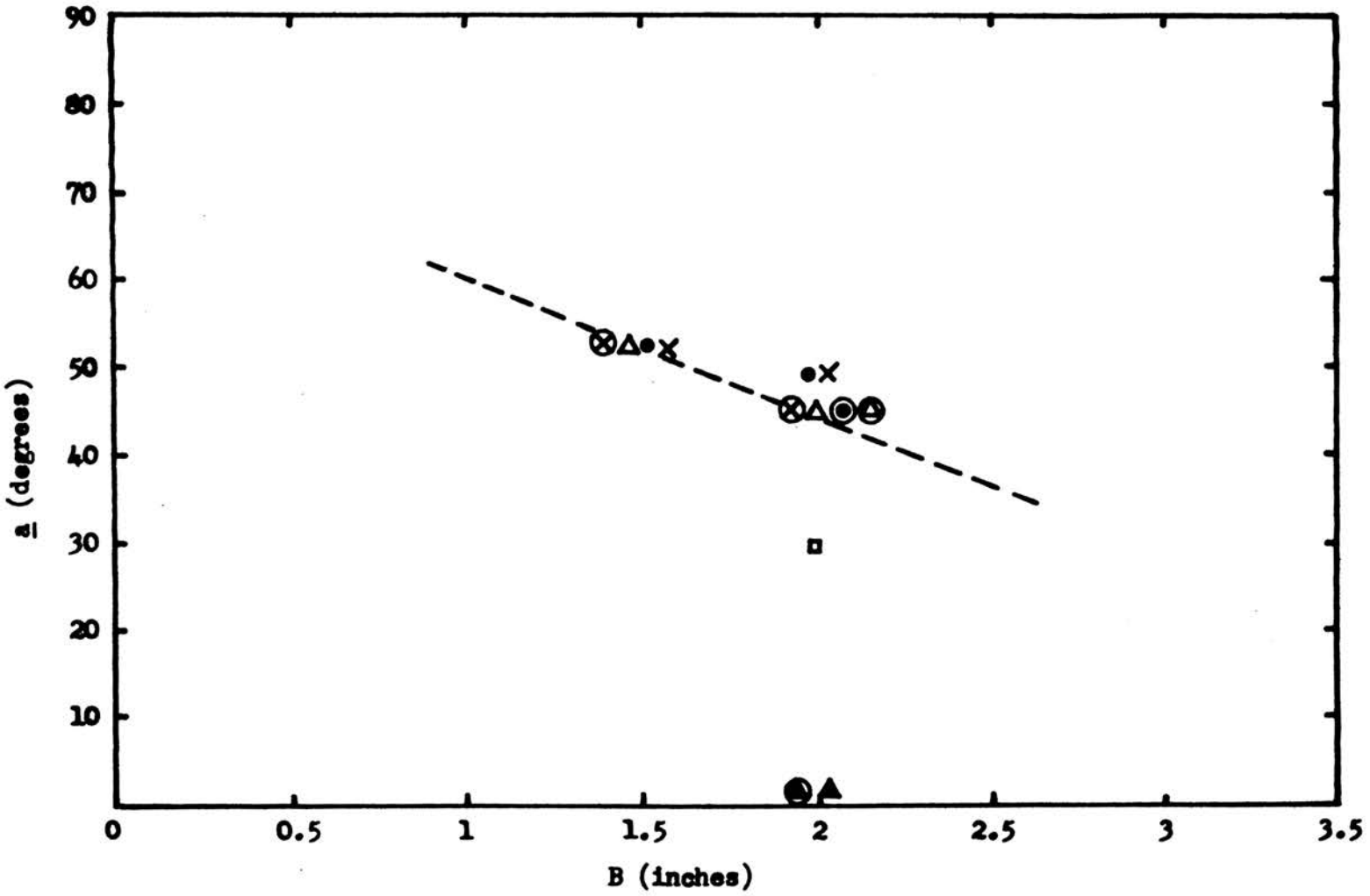

Figure 11. Burden vs. Crater Angle a for Cubes of Hydrostone

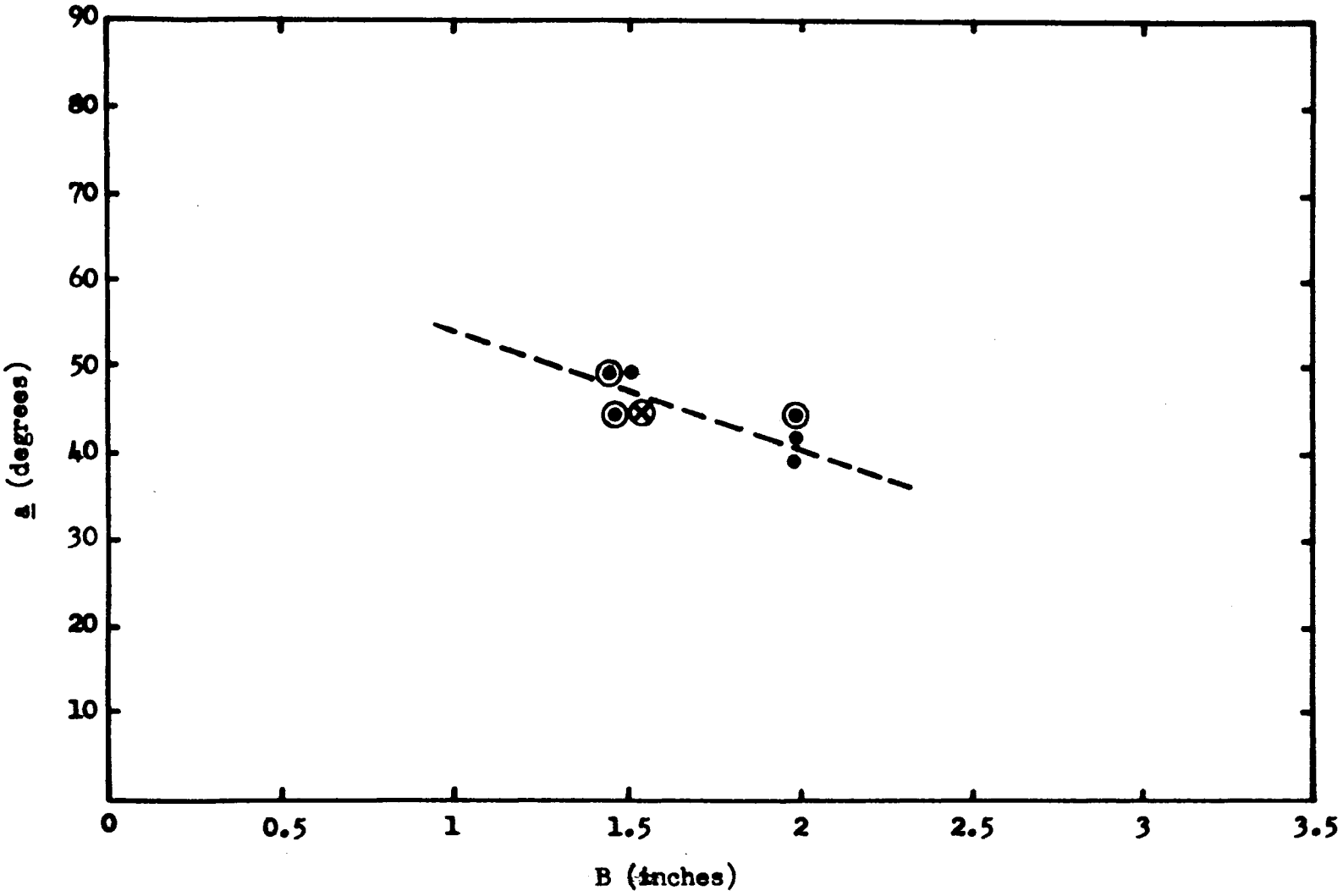

Figure 12. Burden vs. Crater Angle a for Cubes of Dolomite.

2-inch burdens the dolomite and mortar wet specimens broke along wider a angles than did their dry counterparts. Hydrostone, on the other hand, exhibited the opposite tendency, probably due to the fact that Hydrostone wet models absorbed considerably more water than did the dolomite and mortar, i.e., 10 per cent as compared to 3 and 2 per cent, respectively. The presence of water also appeared to intensify stressing at distance, possibly because less energy absorption and scattering occurred (Plates X and XI, XVIII, and XIX). It is interesting to note, however, that a decreased less with increases of burden for the wet samples than it did when they were dry, except in the case of Hydrostone.

The decrease in values of angle a with increased B values was much greater when specimens were tested submerged under water than when air was the surrounding environment. In addition, for most instances no slabs were formed (Plates XX, XXI, XXII, and XXIII), and fracturing of specimens was severely reduced (Plates XI and XXI, XVI and XX). The effects could be attributed possibly to the fact that less of the initial compressive stresses generated by the explosive charges were reflected at the interfaces because of closer impedance matching. When a steel plate was used as the refractive media at one of the free faces, the crater process was noticeably altered (Plates XXIV and XXV). This too would be expected because the compressive stresses on striking the interfaces should have not changed phase on reflection.

Referring to Figure 13 and 14, the influence of the stress wave cone-angle c on crater angle a is clearly shown. From the limited data there appeared to be a general decrease in the value of a with increasing c angles up to about 37 degrees, after which the value of a increased

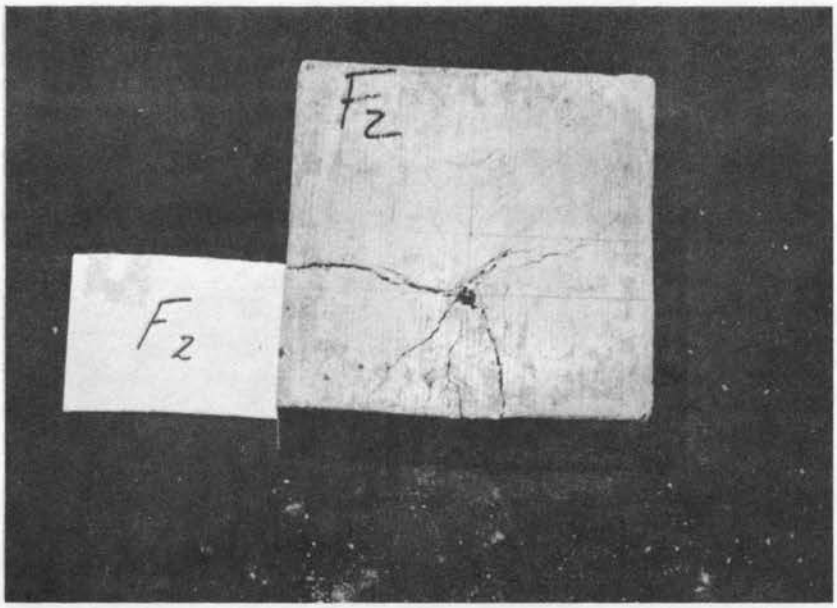

Plate XXI. Dry Cube of Mortar Fired with 2-inch Burden and Water Interfaces.

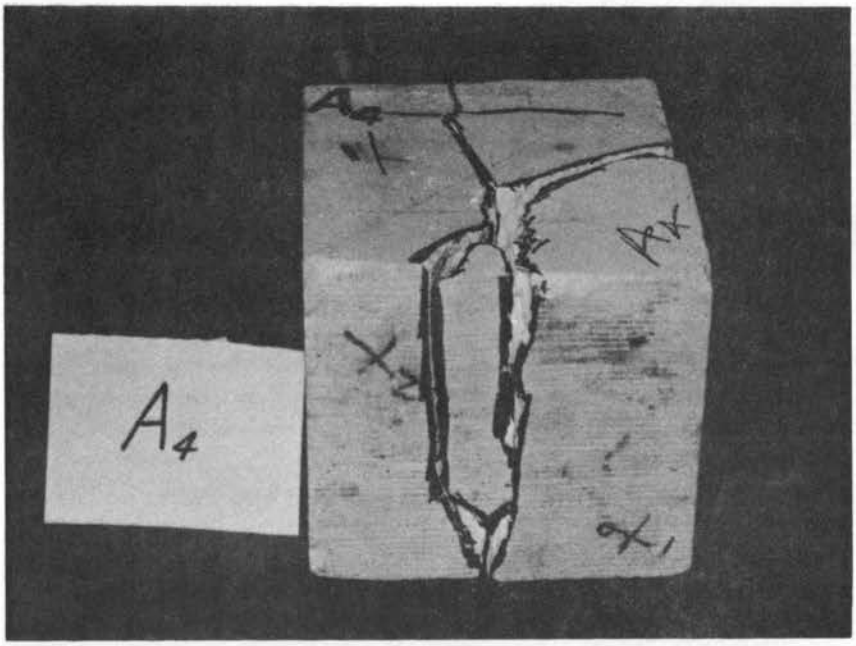

Plate XXII. Wet Hydrostone Fired with 1.5-inch Burden and Water Interfaces.

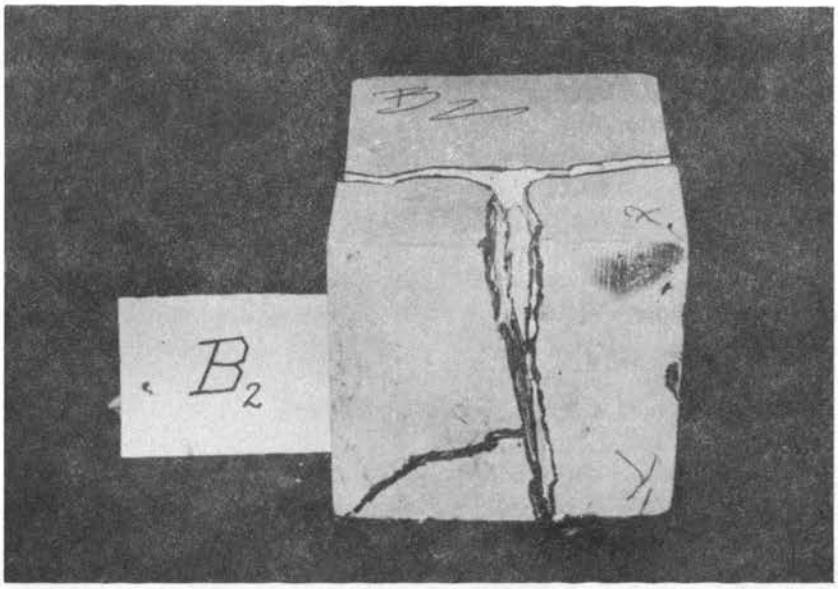

Plate XXIII. Wet Hydrostone Fired with 2-inch Burden and Water Interface.

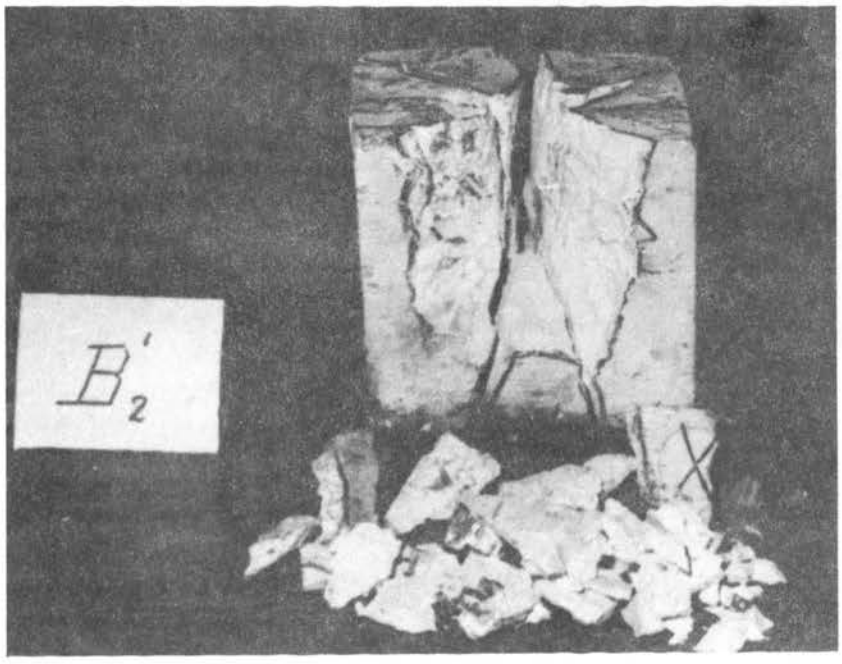

Plate XXIV. Dry Hydrostone Fired with 2-inch Burden and Bottom Face Placed on Steel Plate.

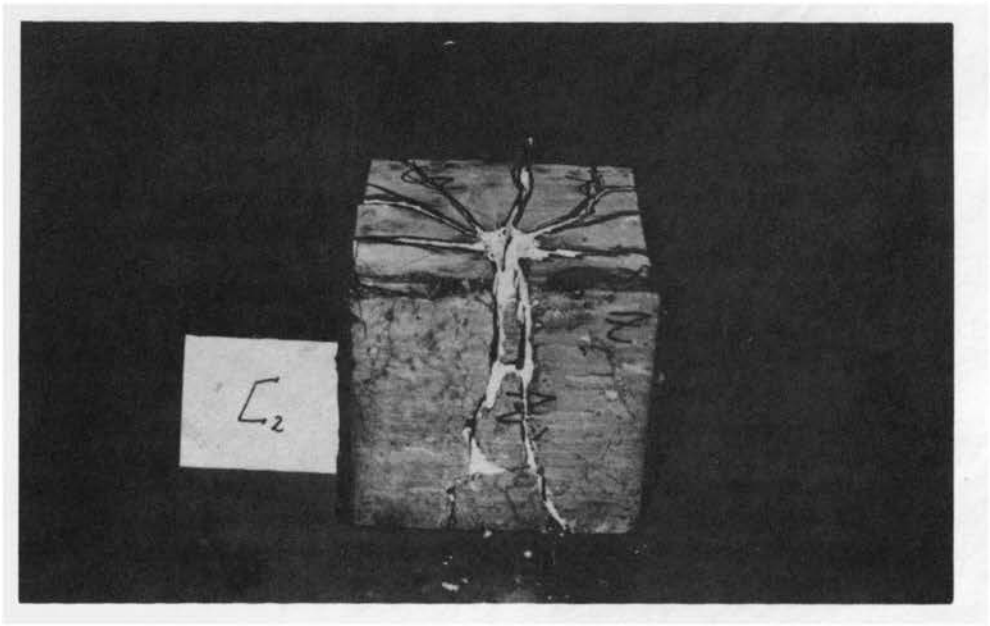

Plate XXV. Dry Hydrostone Fired with 2-inch Burden and Front Face Placed on Steel Plate.

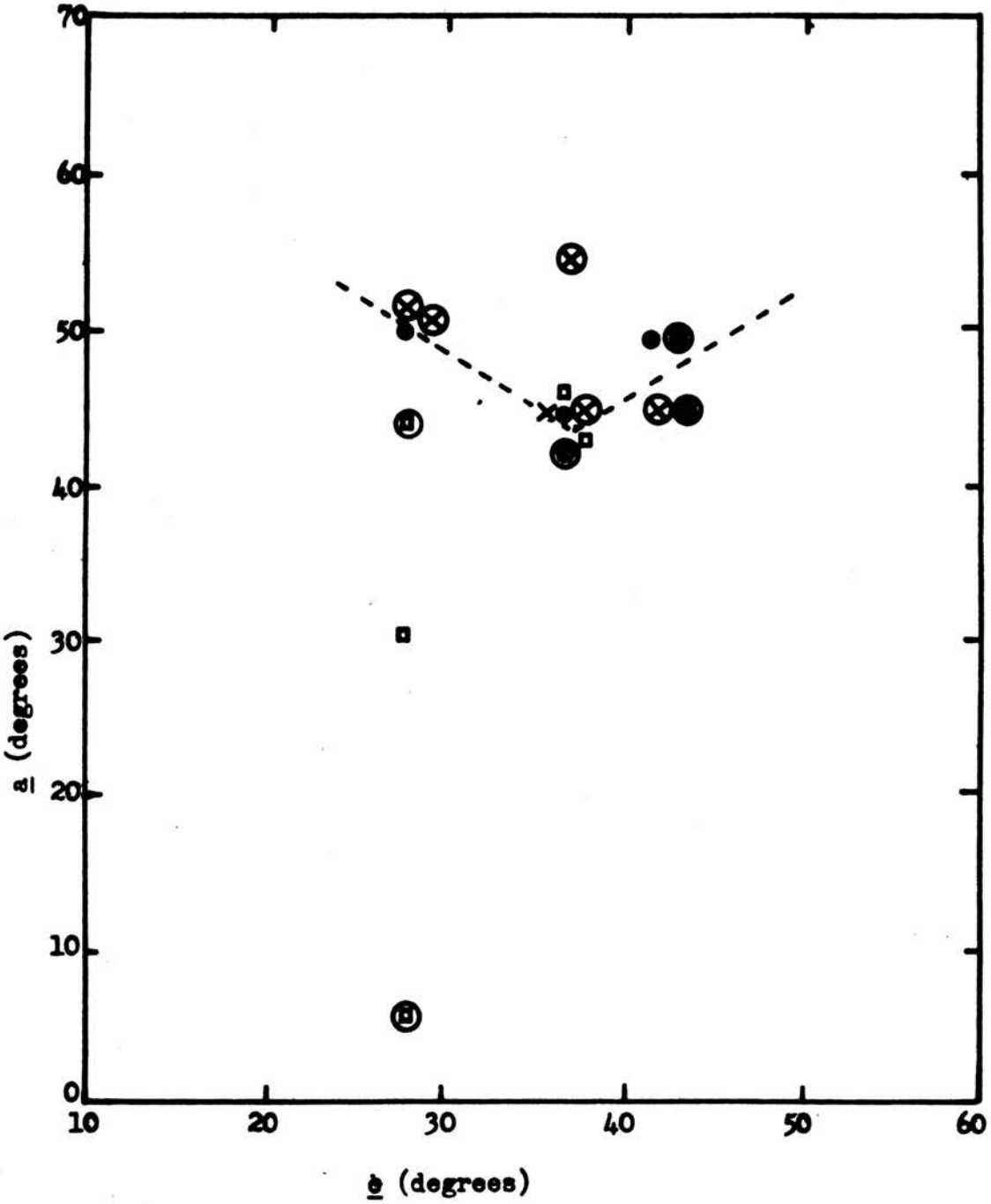

Figure 13. Stress Cone Angle vs. Crater Angle a For Specimens With 1.5-inch Burden.

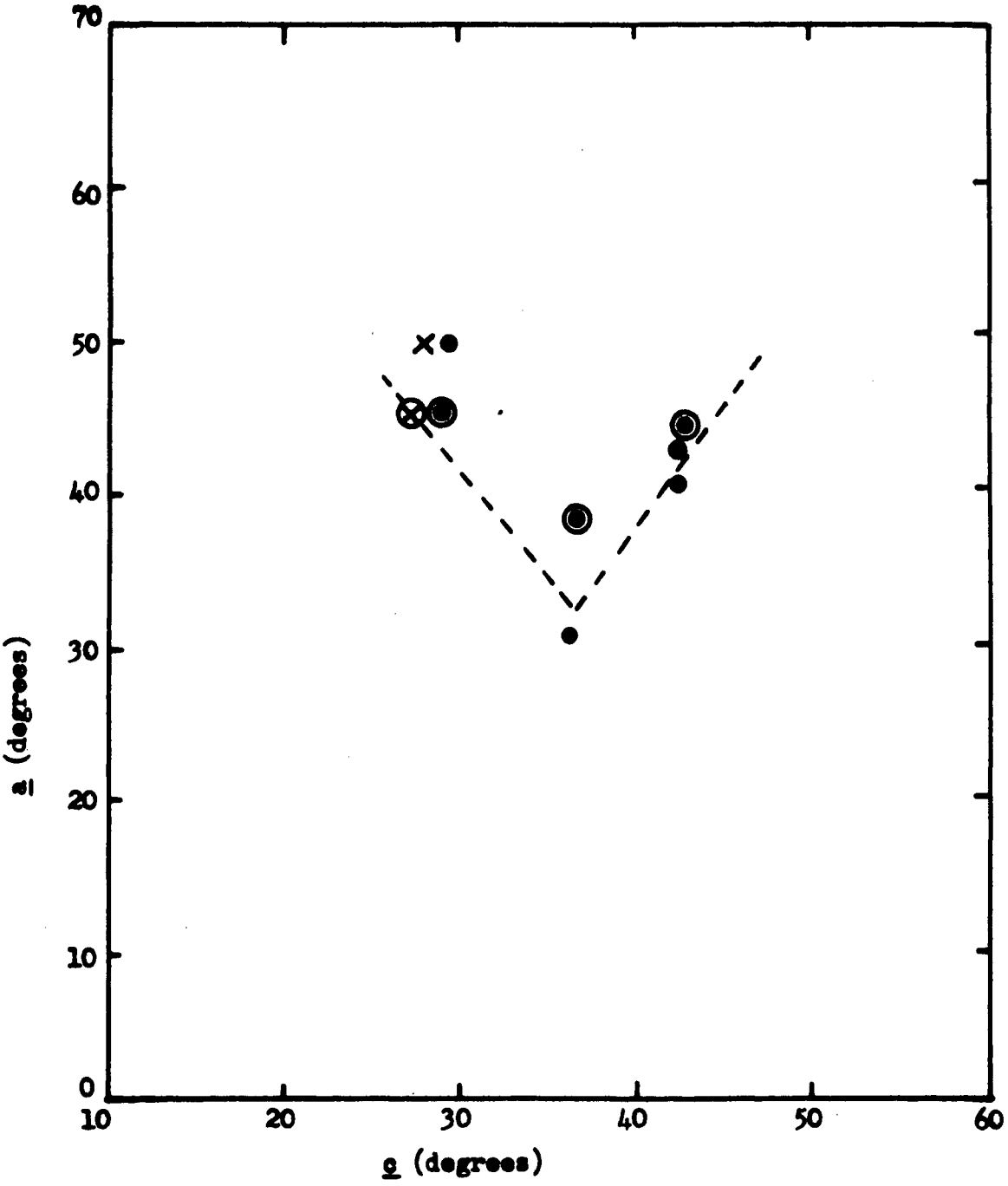

Figure 14. Stress Cone Angle vs. Crater Angle $\underline{a}$ For Specimens With 2-inch Burden.

with higher c angles for specimens tested in an air environment. The changes of angle a with increasing values of c were much greater at the 2-inch than they were for the 1-1/2 inch burdens. On the other hand, referring back to Figures 9, 10, 11, and 12, it was noted that a varied inversely with increasing burdens. Therefore, it would appear that in the range of 35 to 40 degrees for angle c stress conditions may have been transitional. It is significant that the phenomena would have occurred with the mortar specimens for which properties should have been reasonably isotropic. However, the textural properties for the Hydrostone and mortar were fairly uniform while for the dolomite its testure was extremely heterogeneous. Possibly with more uniform specimens with the higher characteristic c value, angle a may have continually reduced as c increased.

On inspection of angle b for craters, and the shape of cones and plugs formed from specimens, it was found that its value was influenced by the stress-wave angle c characteristic of the material tested. Measurements showed that in practically all instances the values of angle b was never less than the characteristic cone angle c for the specific model. In comparing Figures 17, 18, 19, and 20, one finds the value of angle b always decreased for increasing burden dimensions. The most rapid decrease was for the Hydrostone.

It should be noted that the critical region for c values, i.e., between 35 and 40 degrees, found present for angle a, also appeared to exist for angle b. When 1.5-inch burdens were used (Fig. 15), the value of b remained constant at 45 degrees up to the critical range for both dry and wet specimens, beyond which the dry specimens increased

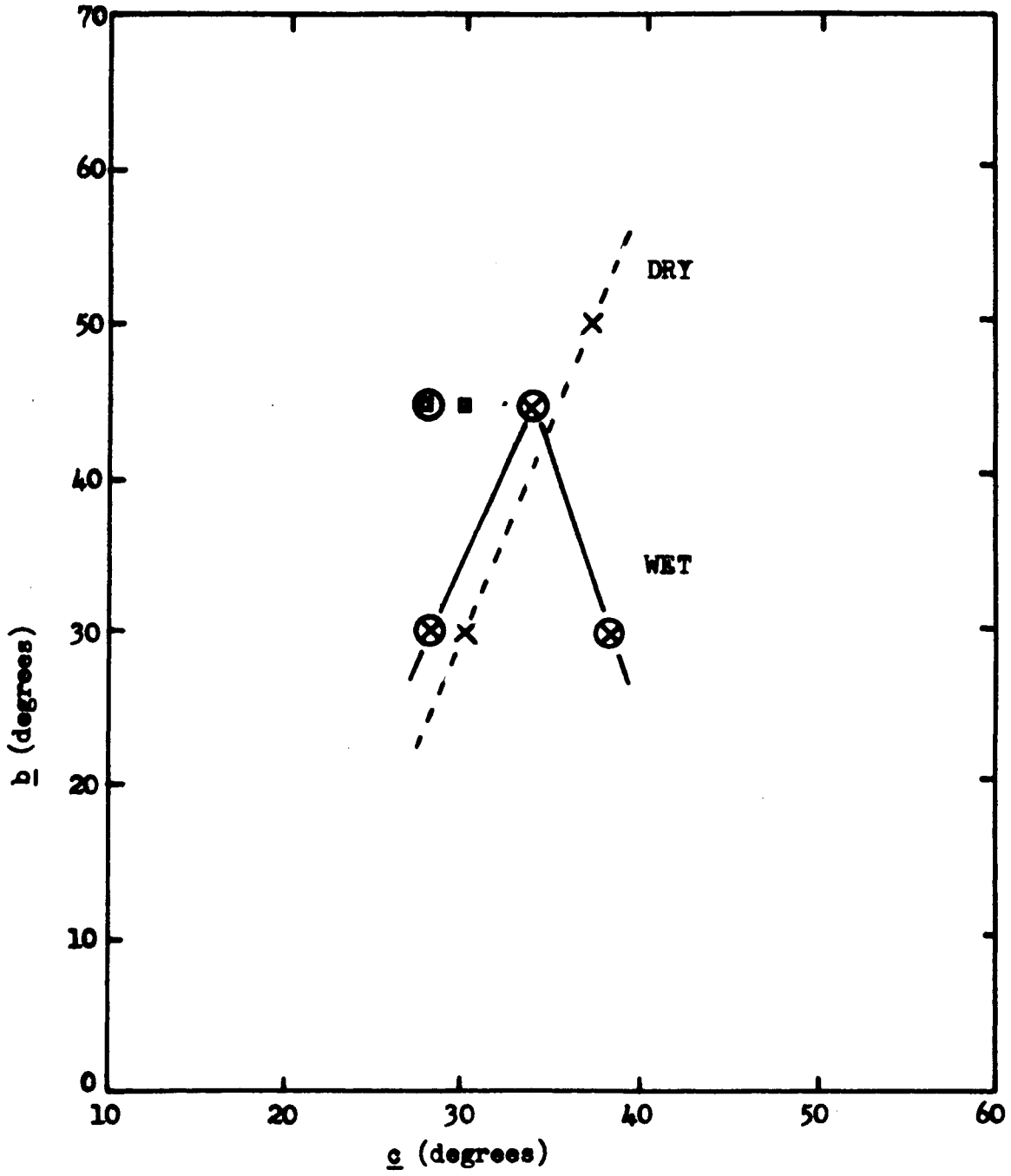

Figure 15. Stress Cone Angle vs. Crater Angle b For Specimens with 2-inch Burden.

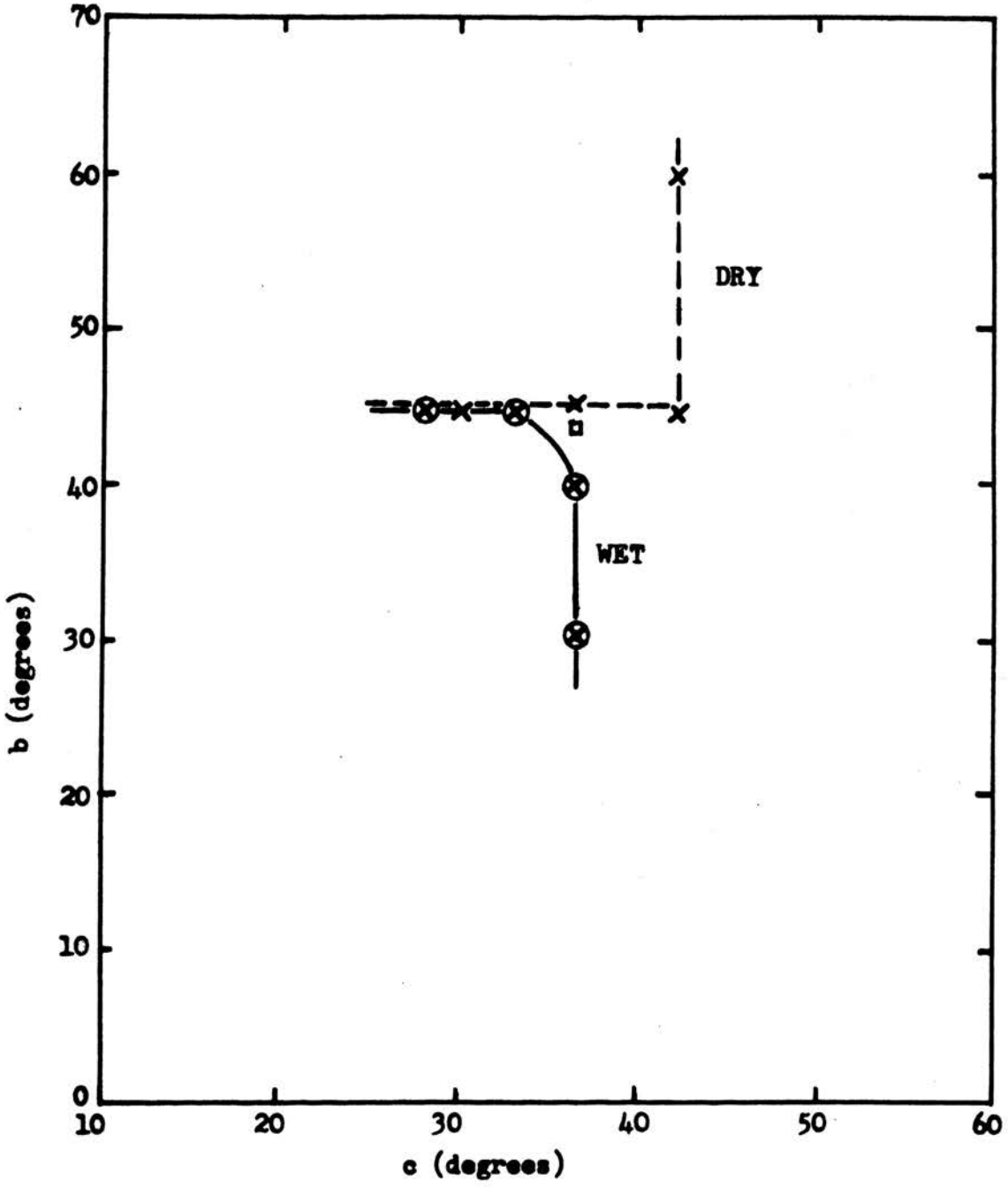

Figure 16. Stress Cone Angle vs. Crater Angle b for Specimens With 1.5-inch Burden.

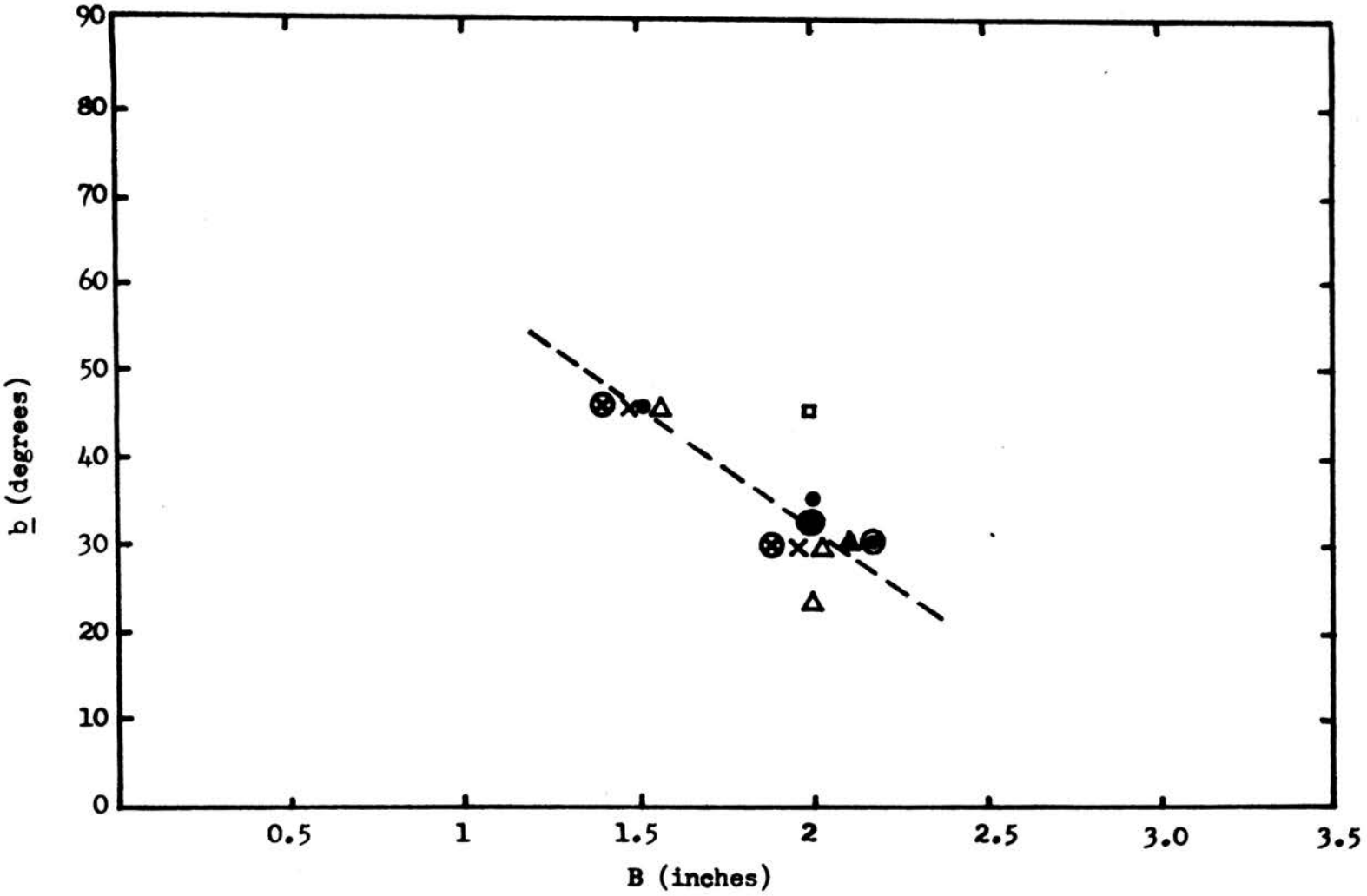

Figure 17. Burden vs. Crater Angle b for Cubes of Hydrostone.

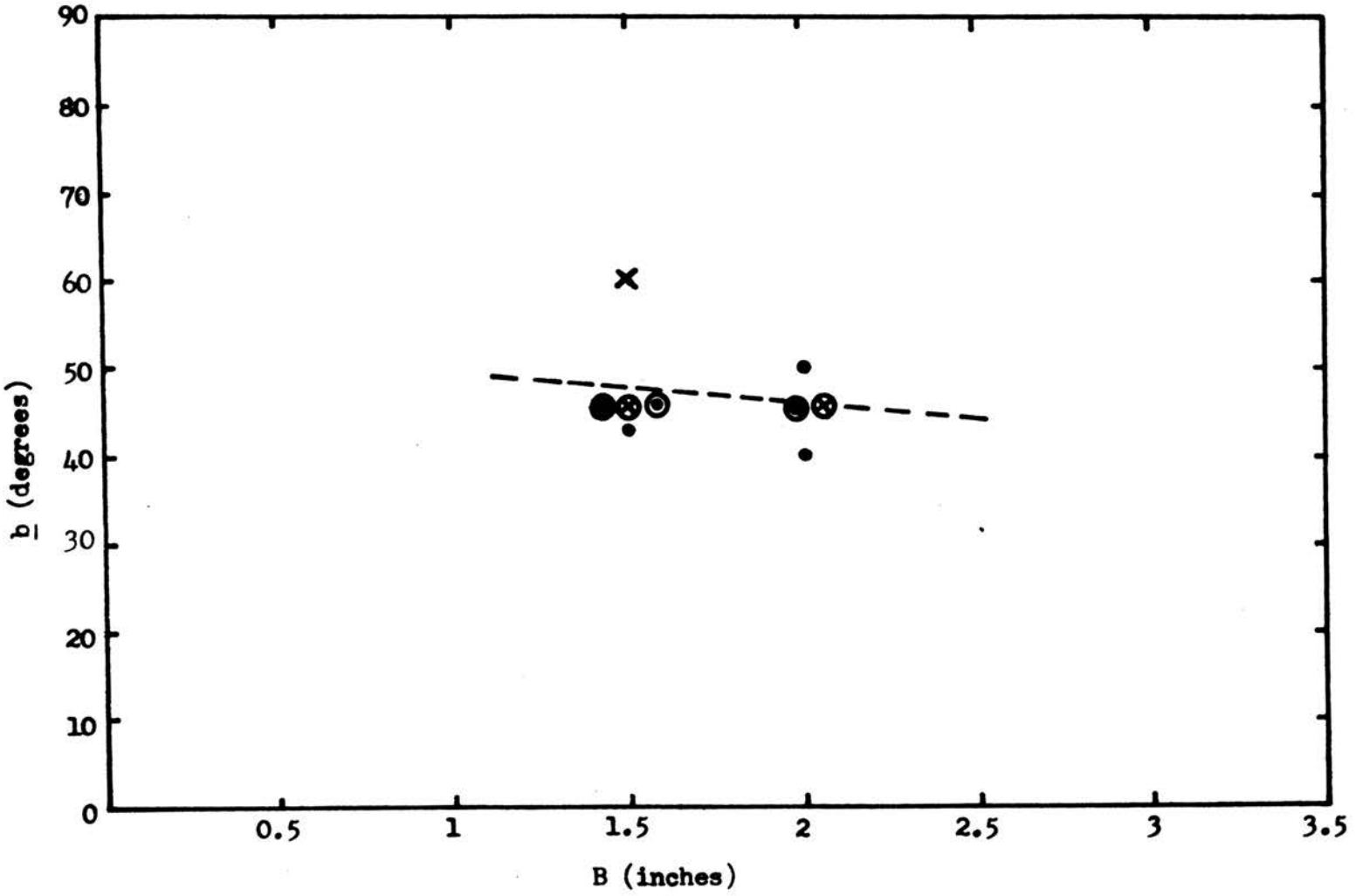

Figure 18. Burden vs. Crater Angle b for Cubes of Dolomite.

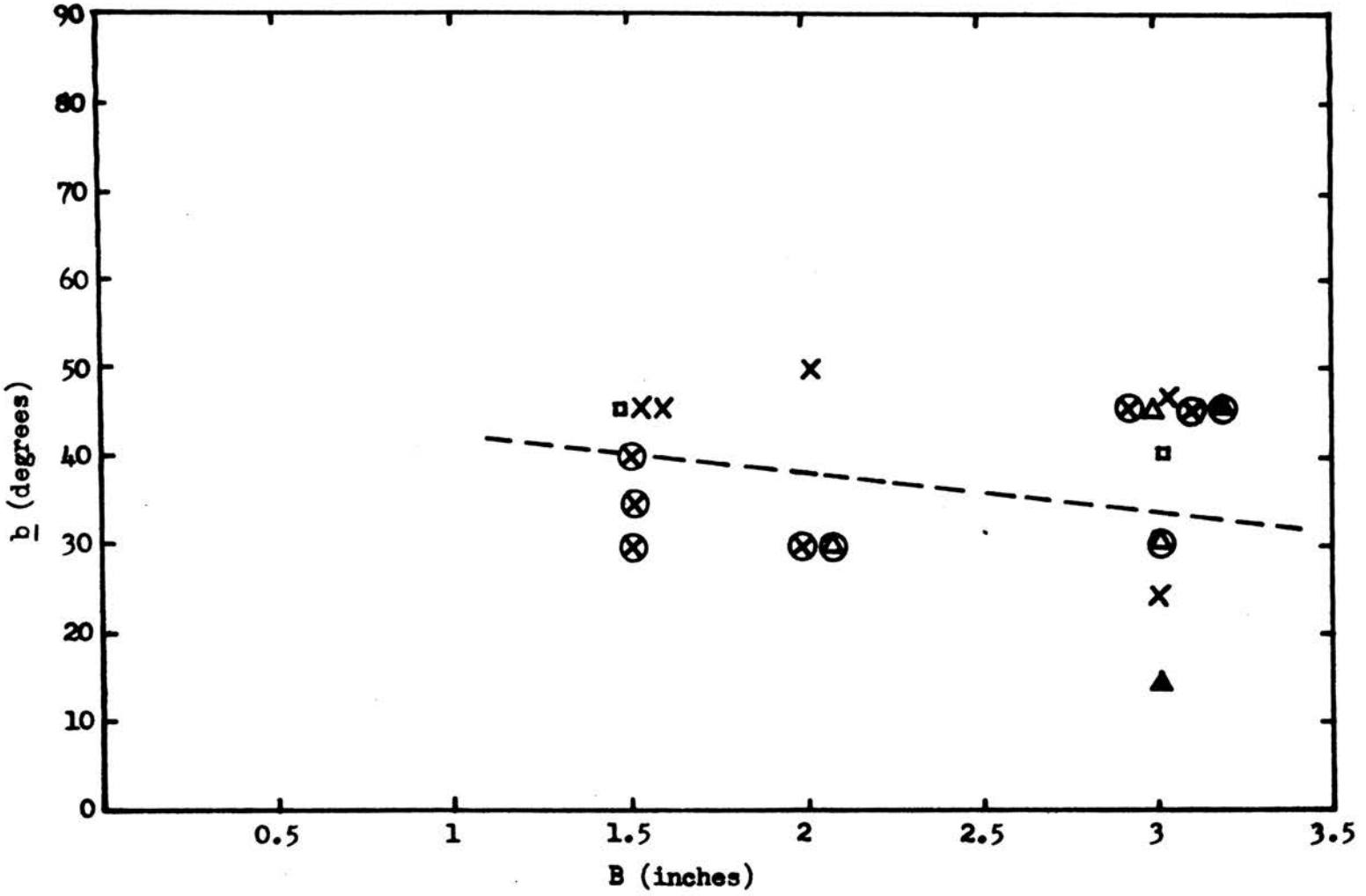

Figure 19. Burden vs. Crater Angle b for Cubes of Mortar.

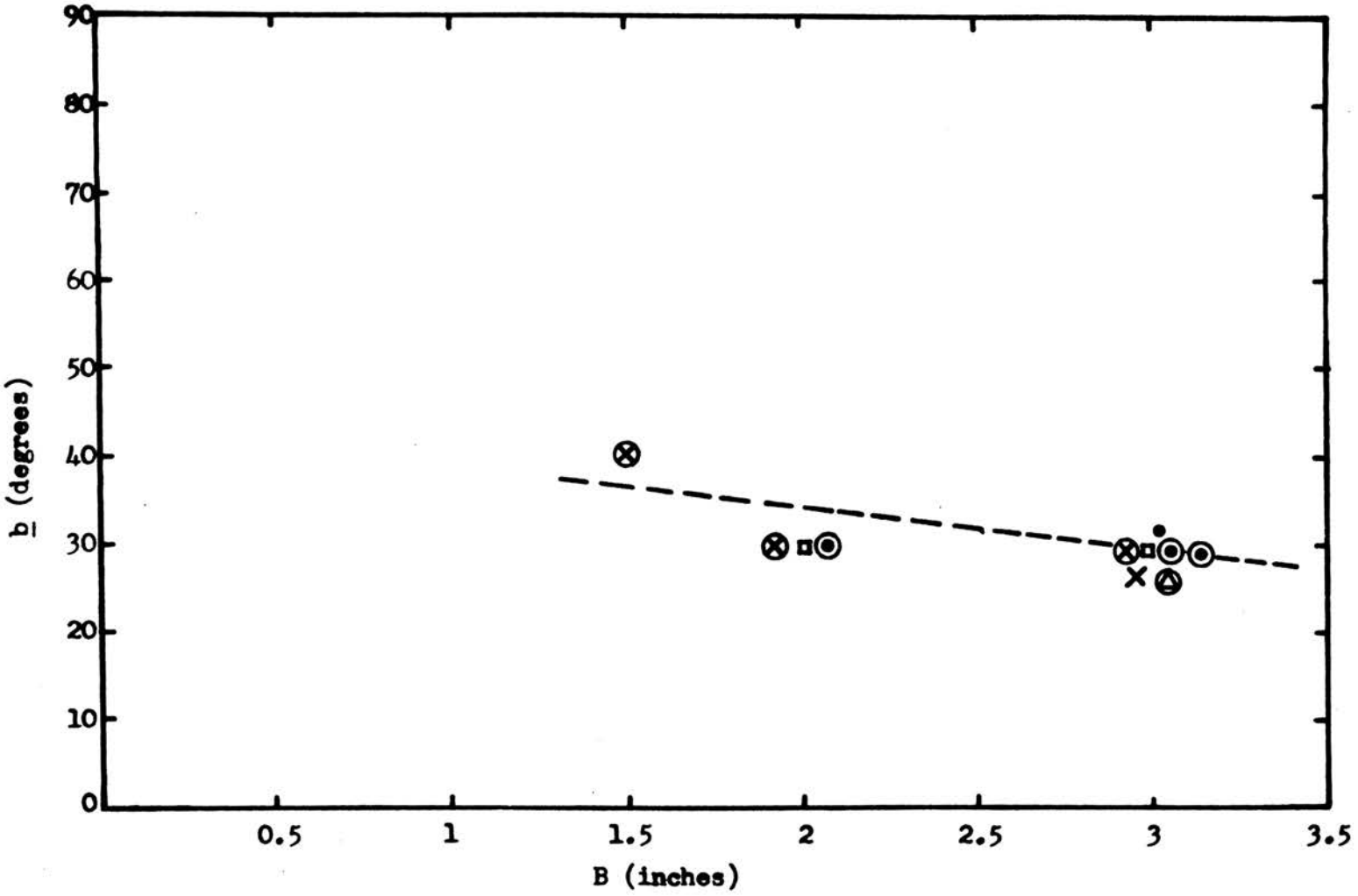

Figure 20. Burden vs. Crater Angle b for Cylinders of Mortar.

their b values while the wet models produced lower values. For 2-inch burdens (Fig. 16), on the other hand, wet specimens increased their b values with increasing c angles up to a maximum of 45 degrees within the critical range, beyond which there appeared a sudden drop of b to near 30 degrees. Dry specimens did not exhibit any change in their proportionate increase of b values with c angle increase.

In reviewing data on Figures 13, 14, 15, and 16, it appears that crater angles a and b as a function of the stress-cone angle c and moisture content are noticeably different when the same burdens were used. The burden had the strongest effect on angle a. The marked change in trends for the two crater angles with cone angle c beyond the 35 to 40-degree range may be particularly significant. Quite likely the difference in angles of incidence in the two planes of the stress cone and the relationship of a material's shear to tensile strength decide the respective crater angles a and b. In addition, the two free faces at the top edge or corner of specimens showed a strong effect on angle a that was absent in the case of angle b. With large burdens edge effects due to the proximity of side free faces tended to eliminate the formation of crater.

V. CONCLUSIONS

Results from this investigation support the following conclusions:

1. End — initiated cylindrical explosive charges, exhibiting steady reaction rates, with L/D ratios greater than 10 generate conical compressive-wave forms in rigid materials, the cone angle of which is defined by the relationship, $\underline{c} = \arcsin V_p/V_e$.
2. The cone angle $\underline{c}$, characteristic of the material being blasted and the explosive used, exerts a significant influence on the three crater parameters: s, angle $\underline{a}$, and angle $\underline{b}$.
3. The presence of water in rock-like materials apparently changes the characteristic Poisson's ratio by raising its value, tending to alter the fracturing mechanisms due to reflection.
4. The angle of incidence, α, of stresses striking impedance interfaces is never less in value than the $\underline{c}$ angle defined by the blasting conditions, except in the vicinity of the charge initiation.
5. The fragment thickness, s, of the crater products is a function of the compressive wave amplitude propagated by the charge, the accoustical match of the two media bounding an interface, and the stress incidence angle, α, the lowest value of which is equal to the stress-cone angle $\underline{c}$.
6. The fragment thickness has an inverse relationship with the burden dimension and a direct relation with the impedance difference at discontinuities.
7. Craters can be formed from detonating explosives without the development of slabs, implying that initial fracture mechanisms are not dependent solely on reflected tensile stresses and could be formed by either shear or tension, or a combination of both.

8. Cylindrical or round-faced models develop greater crater angles a than do those with cubic or flat-faced shapes.

9. The crater angles a and b follow different inverse relationships with the same burden dimension.

10. A transition zone exists for materials with characteristic angles of c, which for the materials tested was found to be between 35 and 40 degrees. In this region, angles a and b exhibit reverse trends in their otherwise normal general effects.

11. The value of angle b for craters, and for cones or plugs characteristic of crater forms, produced by long cylindrical explosive charges in rock materials appears to be never less in value than the characteristic stress-cone angle c.

12. The inclusion of water within a material decreases the attenuation of explosive energy.

13. Underwater blasting severely reduces rock fracturing effects, impeding the formation of slabs in the mechanism of cratering.

14. Refractive materials at interfaces with much higher accoustical impedances than the material being blasted will severely reverse the effect of stress-wave energy in crater development.

VI. RECOMMENDATIONS FOR FURTHER STUDY

Confirmation of conical stress waves shown to exist by this investigation, which occur when the explosive's reaction velocity exceeds the P-wave velocity characteristic of a medium or when multiple priming is utilized with detonating fuse as the initiator, should have a real significance on blast effects for many open pit mines, underground mines using long-hole blasting, and quarry operations with high ledges. However, information from these studies and the literature for both conical and spherical stress waves is not yet adequate to properly define relationships between explosives' and materials' properties for purpose of design, particularly in regard to multiple-hole blasting. For these reasons, therefore, it is recommended that additional research be conducted in the following areas for both the conical and spherical stress-wave conditions:

1. A mathematical solution for a conical stress wave should be developed.
2. The role of stemming length on the distribution of stresses in the collar region of a blasthole should be clearly defined.
3. A determination in regard to the function of subdrilling on the fracture mechanisms of rock located at floor level in bench blasting should be made.
4. The role of geologic structure on the dynamic stressing of rock by explosives should be ascertained.
5. The characteristic stress mechanics involved at the collar and toe of inclined blastholes in benching should be distinguished from those of vertical holes.
6. Optimum limits should be established for charge length dependent

on primer location for any given set of blasting conditions.

7. Relationships between charge spacing as a function of charge length for adjacent blastholes when initiated simultaneously should be determined.

8. The influence of water content in rocks on their elastic properties should be thoroughly investigated.

9. Comparisons should be conducted between the volumes of craters produced by long-length charges and those given by the cube root law normally used for crater studies.

10. Thorough study of the influence of the conical wave on the value of optimum burden dimensions for various materials should be undertaken.

11. Mathematical relationships should be developed for long cylindrical charges where the explosive's reaction velocity equals or is less than the P-wave velocity characteristic of a medium.

12. Detailed analyses of correlations between a material's strengths and the stress cone angle on the parameters of craters produced should be performed.

APPENDIX I.

LIST OF ABBREVIATIONS AND SYMBOLS

A. Abbreviations.

$\underline{a}$	Crater angle in plane of charge diameter, D (deg).
α	Angle of incidence of a stress-pulse at an impedance discontinuity, (deg).
α_p	Angle of the reflected P-pulse (deg).
α_s	Angle of the reflected S-pulse (deg).
Ap	Amplitude of an incident longitudinal stress.
As	Amplitude of incident shear stress.
Ap_1	Amplitude of reflected longitudinal stress.
As_1	Amplitude of reflected transverse stress.
Ap_2	Amplitude of refracted longitudinal stress.
As_2	Amplitude of refracted shear stress.
$\underline{b}$	Crater angle in plane of charge length, L, (deg).
B	Burden dimension (in.).
β_p	Angle of refracted P-pulse (deg).
β_s	Angle of refracted S-pulse (deg).
$\underline{c}$	Stress wave angle in plane of charge length, L, (deg).
d_e	Density of explosive (pcf).
d_m	Density of material (pcf).
D	Charge diameter (in.).
g	Gravity acceleration constant, equal to 32.2 fps.
L	Charge length (in.).
ρ_1	Mass density of material (lb-sec^2/ft^4).

APPENDIX I.

(Continued)

ρ_2	Mass density of environment (lb-sec^2/ft^4).
s	Slab thickness (in.).
σ_c	Compressive stress of specimen (psi).
σ_t	Tensile strength of specimen (psi).
τ_s	Shear strength of specimen (psi).
μ	Poisson's ratio.
Ve	Reaction Velocity of the explosive (fps).
Vp	Longitudinal wave velocity of a material (fps).
Vs	Shear wave velocity of a material (fps).
W	Weight of the sample (Kg).
z	Accoustical impedance (ps/cf).

B. Symbols for Plotting Experimental Data.

●	Dry specimens with a concrete interface on bottom and air surrounding all other faces.
×	Dry specimens with air surrounding all faces.
▲	Dry specimens with a steel plate on bottom and air surrounding all other faces.
▲	Dry specimens with a steel plate on front face and air surrounding all other faces.
◘	Dry specimens submerged under water.
◉	Wet specimens with a concrete interface on bottom and air surrounding all other faces.
⊗	Wet specimens with air surrounding all faces.
⊜	Wet specimens with a steel plate on bottom and air surrounding all other faces.

APPENDIX I.

(Continued)

- Wet specimens with a steel plate on front face and air surrounding all other faces.
- Wet specimens submerged under water.

APPENDIX II.

SPECIFIC GRAVITY MEASUREMENTS

A. Mortar.

Sample	Weight (gm)	Volume (cc)	Specific Gravity
1	11.24	5.5	2.10
2	10.29	4.0	2.56
3	6.35	3.0	2.10
4	3.85	1.9	2.03
5	5.70	2.6	2.20
6	3.97	2.0	2.00
7	9.00	3.6	2.50

Mean Value: 2.2

B. Dolomite.

Sample	Weight (gm)	Volume (cc)	Specific Gravity
1	2.45	1.0	2.45
2	11.19	4.0	2.49
3	8.95	3.5	2.56
4	8.82	3.5	2.53
5	2.15	0.9	2.44
6	2.51	1.0	2.52
7	15.08	6.0	2.50

Mean Value: 2.5

APPENDIX III.

V_p MEASUREMENTS

A. Dry Mortar.

Sample	Axis	Length (in.)	Travel Time (μ sec.)	V_p (fps)
A_3	x	5.812	36.5	13,268
	y	5.860	36.5	13,378
	z	5.643	38.0	12,375
C_3	x	5.816	36.0	13,467
	y	5.828	36.0	13,492
	z	5.820	36.5	13,292
E_3	x	5.942	38.0	13,033
	y	5.955	38.0	13,058
	z	5.954	37.0	13,410
	x	5.900	36.5	13,470
	y	5.750	36.5	13,128
	z	5.937	36.0	13,743
G_3	x	5.858	36.5	13,374
	y	5.783	36.5	13,203
	z	5.765	36.5	13,162
C_2	cyl.	5.850	39.0	12,500
B_2	cyl.	5.938	39.5	12,527
D_4	cyl.	6.030	38.0	13,224
A_4	cyl.	6.125	38.5	13,258

Maximum:	13,743
Minimum:	12,375
Values above 13,000	16
Values below 13,000	3
Approximate Mean:	13,200 fps

APPENDIX III.

(continued)

B. Wet Mortar.

Sample	Axis	Length (in.)	Travel Time (μ sec.)	V_p (fps)
A_3	x	5.812	36.5	13,280
	y	5.860	37.0	13,200
	z	5.643	35.5	13,200
C_3	x	5.816	36.0	13,480
	y	5.828	36.0	13,500
	z	5.820	36.0	13,300
E_3	x	5.942	37.0	13,380
	y	5.955	38.0	13,070
	z	5.954	36.0	13,800
J_3	x	5.900	36.5	13,480
	y	5.750	36.0	13,300
	z	5.937	37.0	13,320
G_3	x	5.858	36.0	13,580
	y	5.783	36.0	13,380
	z	5.765	36.5	13,200
C_2	cyl.	5.850	35.0	13,900
B_2	cyl.	5.938	38.5	12,800
D_4	cyl.	6.030	37.0	13,550

Maximum:	13,900
Minimum:	12,800
Values above 13,000:	17
Values below 13,000:	1

Approximate Mean: 13,300 fps

APPENDIX III.

(continued)

C. Dry Dolomite.

Sample	Axis	Length (in.)	Travel Time (μ sec.)	V_p (fps)
10	x	5.454	30.0	15,200
	y	6.951	40.0	14,500
	z	5.518	30.0	15,300
12	x	4.785	25.0	16,000
	y	6.195	38.0	13,600
	z	5.603	34.0	13,900

Maximum: 16,000
Minimum: 13,600
Values above 14,000: 4
Values below 14,000: 2

Approximate Mean: 14,800 fps

D. Wet Dolomite.

Sample	Axis	Length (in.)	Travel Time (μ sec.)	V_p (fps)
G_2	x	6.938	47.0	12,000
	y	5.563	38.0	12,400
	z	5.250	34.0	12,900
F_1	x	6.938	50.0	11,550
	y	7.282	52.0	11,680
	z	9.844	66.0	12,400

Maximum: 12,900
Minimum: 11,550
Values above 12,000: 4
Values below 12,000: 2

Approximate Mean: 12,200 fps

APPENDIX III.

(continued)

E. Dry Hydrostone.

Sample	Axis	Length (in.)	Travel Time (μ sec.)	V_p (fps)
A_2^1	x	6.035	45.5	11,020
	y	5.965	45.0	11,050
	z	5.930	44.5	11,100
A_4^1	x	6.025	45.0	11,200
	y	6.013	46.0	10,900
	z	5.929	45.0	11,000
A_3^1	x	5.867	45.0	10,850
	y	5.736	45.0	10,600
	z	5.792	45.0	10,700
B_1^1	x	5.899	43.5	11,280
	y	5.714	43.0	11,100
	z	5.797	44.0	10,900
B_2^1	x	5.993	44.5	11,200
	y	5.866	43.0	11,370
	z	5.800	43.5	11,100

Maximum:	11,370
Minimum:	10,600
Values above 11,000:	10
Values below 11,000:	5
Approximate Mean:	11,000 fps

APPENDIX III.

(continued)

F. Wet Hydrostone.

Sample	Axis	Length (in.)	Travel Time (μ sec.)	V_p (fps)
A_4	x	5.922	48.5	10,170
	y	5.769	48.5	9,920
	z	5.860	48.5	10,070
B_1	x	5.745	48.0	9,970
	y	5.945	48.0	10,300
	z	5.787	47.5	10,160
B_2	x	5.833	48.5	10,000
	y	5.970	47.5	10,480
	z	5.750	47.5	10,080

Maximum:	10,480
Minimum:	9,920
Values above 10,000:	7
Values below 10,000:	2
Approximate Mean:	10,200 fps

APPENDIX IV.

EXPERIMENTAL DATA

Note: (10) Tested with 20-gr MDF
(x) Steel plate against vertical face opposite burden

A. Dry Mortar Cubes.

Burden (in.)	Environment	Sample	W (Kg)	Water Cont. (%)	2a (deg.)	b (deg.)	s (in.)	Comments
3	Concrete	B_2 (10)	7.627	---	----	----	----	Specimen did not split apart.
		D_2 (10)	7.547	---	----	----	----	Radial fractures oriented towards free faces.
	Air	G_1	7.655	---	60	45	0.5	Conic plug was ejected at the bottom. Specimen was shot upside down.
		I_2	7.690	---	----	25	----	Specimen broken in 3 pieces, but showed trend to break in 4 pieces.
	Steel	B_3 (10)	6.696	---	----	----	----	Specimen was barely cracked.
		D_3 (10)	6.963	---	----	----	----	Results similar to B_3.
		E_1 (x)	7.813	---	----	15	----	No slabbing present.
		J_1	7.883	---	75	45	----	The angle a was formed towards the nearest free face, due to the hole being slightly excentrical.

APPENDIX IV.

(Continued)

Burden (in.)	Environment	Sample	W (Kg)	Water Cont. (%)	2a (deg.)	b (deg.)	s (in.)	Comments
3	Water	I_3	6.964	---	---	40		Specimen broken in 4 pieces. No slabbing.
2	Concrete	A_2	7.616	---	60	50	0.5 to 0.6	Good example of crater formation, clear slabbing.
	Water	C_2	7.586	---	---	---	---	Crater was not ejected. Angle a was recorded examining breaking trends.
		F_2	7.786	---	---	---	---	Similar to C_2
1.5	Concrete	H_2	7.950	---	90	45	0.5	----
	Air	H_1	7.918	---	90	45	0.5	Good cratering
	Water	C_1	7.764	---	80	---	---	Almost no back fracturing
		F_1	7.938	---	80	45	---	Crater ejected with no slabbing indication.

APPENDIX IV.

(Continued)

B. Wet Mortar Cubes.

Burden (in.)	Environment	Sample	W (Kg)	Water Cont. (%)	2a (deg.)	b (deg.)	s (in.)	Comments
3	Concrete	A_1 (10)	7.585	2.4	90	---	---	Radial cracks extending toward free-faces.
		D_1 (10)	7.758	2	90	---	---	All radial fractures reach the free faces but they run only halfway downwards.
	Air	G_2	7.777	2.7	60	45	0.5 to 0.6	-----
		I_1(10)	7.964	1.6	65	45	---	Crater was not ejected but angle a was clearly shown.
	Steel	E_2 (x)	7.885	1.4	80	45	---	Angle a was measured towards the face opposite the steel plate.
		J_2	7.820	1.2	90	30	---	Top surface showed very good fragmentation.

APPENDIX IV.

(Continued)

Burden (in.)	Environment	Sample	W (Kg)	Water Cont. (%)	2a (deg.)	b (deg.)	s (in.)	Comments
2	Concrete	A_3	6.949	2.1	75	30	0.5 to 0.6	----
	Steel	C_3	7.177	1.7	90	30	0.5 to 0.6	Good example of cratering mechanism. Contact between steel and specimen was not perfect because of uneven surface of the specimen.
1.5	Concrete	E_3	7.553	1.9	85	35	0.5	---
	Air	G_3	7.064	2.0	90	30	0.5	---
		J_3	7.341	1.8	110	40	0.5 to 0.6	Good slabbing.

APPENDIX IV.

(Continued)

C. Dry Mortar Cylinders.

Burden (in.)	Environment	Sample	W (Kg)	Water Cont. (%)	2a (deg.)	b (deg.)	s (in.)	Comments
3	Concrete	C_1 (10)	5.402	---	95	30	0.4	3 pie-shaped fragments.
		D_3	6.032	---	---	---	0.4	Clear slabbing.
		D_1 (10)	6.034	---	50	---	0.4	6 pie-shaped fragments.
	Air	A_5	6.058	---	70	30	0.5	Clear slabs.
		C_6	5.463	---	---	---	---	No slabbing, fracturing was very erratic.
	Steel	B_5 (10)	5.983	---	90	---	---	4 pie-shaped fragments, no slabbing.
	Water	C_3	5.457	---	60	---	---	6 pie-shaped fragments.
		D_6	6.025	---	60	30	---	A great trend to break in 6 pie-shaped fragments was evidenced.
2	Concrete	A_3	5.969	---	100	30	0.4 to 0.5	A good example of crater formation. Clear slabbing.

APPENDIX IV.

(Continued)

D. Wet Mortar Cylinders.

Burden (in.)	Environment	Sample	W (Kg)	Water Cont. (%)	2a (deg.)	b (deg.)	s (in.)	Comments
3	Concrete	C_4	5.738	4.3	60	30	---	6 pie-shaped fragments.
		D_5	6.136	1.8	40	30	0.5	9 well defined pie-shaped fragments. Clear slabbing.
		D_2	6.175	2	60	---	---	Trend to form 6 pie-shaped fragments but only 5 are clearly defined.
	Air	A_6	6.191	2	30	30	0.4 to 0.5	Top surface very badly fractured.
		C_5	5.658	5	---	---	0.6	Best fragmentation obtained. Clear slabbing.
	Steel	B_6	6.180	1.9	60	30	0.5	Clear slabs. 6 pie-shaped fragments obtained.
2	Concrete	D_4	6.135	2.2	90	30	0.5	----
	Air	C_2	5.732	4	100	30	0.5	Good slabs.
1.5	Air	B_2	6.170	1.8	120	40	0.5	----

APPENDIX IV.

(Continued)

E. Dry Jefferson City Dolomite.

Burden (in.)	Environment	Sample	W (Kg)	Water Cont. (%)	2a (deg.)	b (deg.)	s (in.)	Comments
2	Concrete	B_1	8.656	---	80	50	---	Badly fractured. Slabs appear, but thickness vary widely.
		E_1	9.157	---	85	40	---	Fractured in big fragments, no slabs.
	Air	D_1	9.371	---	85	---	---	No b angle. Poor fragmentation, no slabs.
1.5	Concrete	C_1	8.704	---	100	45	0.7 to 0.8	Good fragmentation. Sample very altered.
	Air	A_1	9.096	---	100	60	0.4 to 0.6	Good fragmentation, clear slabbing.

APPENDIX IV.

(Continued)

F. Wet Jefferson City Dolomite.

Burden (in.)	Environment	Sample	W (Kg)	Water Cont. (%)	2a (deg.)	b (deg.)	s (in.)	Comments
2	Concrete	B_2	9.645	2.6	90	45	0.4 to 0.5	Clear slabbing.
	Air	D_2	10.110	2.7	110	45	0.6	Good fragmentation, clear slabbing.
1.5	Concrete	A_2	8.474	3.5	90	45	---	Specimen was excessively fractured.
		C_2	10.512	3.8	100	45	0.3 to 0.5	
	Air	E_2	9.416	2.6	90	45	0.4 to 0.5	----

APPENDIX IV.

(Continued)

G. Dry Hydrostone.

Burden (in.)	Environment	Sample	W (Kg)	Water Cont. (%)	2a (deg.)	b (deg.)	s (in.)	Comments
2	Concrete	A_3^1	5.056	---	100	35	0.8	Good fragmentation.
	Air	B_1^1	5.501	---	100	30	1.0	---
	Steel	B_2^1	5.149	---	90	30 to 45	0.6	---
		C_2 (x)	5.649	---	0	30	---	Crater thrown in reverse with angle a of 90 deg. - no slabs.
	Water	C_1	5.813	---	60	45	---	Water offered a great resistance to the formation of a crater.
1.5	Concrete	C_4	5.902	---	105	45	0.8 to 1.0	b was shown very clear.
	Air	C_3	5.862	---	105	45	0.6	No back fractures noted.
	Steel	A_1^1	5.918	---	105	30	0.8	---

APPENDIX IV.

(Continued)

H. Wet Hydrostone.

Burden (in.)	Environment	Sample	W (Kg)	Water Cont. (%)	2a (deg.)	b (deg.)	s (in.)	Comments
2	Concrete	A_1	5.719	10.4	90	30	1.0	No back fractures occurred. Slab thickness very clear.
	Air	A_2	5.714	8.6	90	30	---	Fractures went all the way to free faces dividing the specimen in big pieces.
	Steel	A_3	5.840	5.7	90	20 to 25	0.7 to 0.8	A good example of crater formation, clear slabbing.
		B_1 (x)	5.817	11.7	0	30	---	Crater was reversed with an angle a of 90°, no slabbing.
	Water	B_2	5.914	11.4	10	45	---	Apparent narrow crater, no slabbing.
1.5	Air	A_2^1	6.183	9	105	45	0.5 to 0.6	----
	Water	A_4	5.974	9.5	90	---	---	Irregular fracturing, no slabbing. Crater tried to form but was not ejected.

REFERENCES

1. ASH, R. L. (1963). The Mechanics of Rock Breakage, Parts I, II, and IV; Pit and Quarry, Vol. 56, Nos. 2, 3, and 5; August, September, and November.

2. BAUER, A. (1961). Application of the Livingston Theory; Quarterly, Col. Sch. of Mines, Vol. 56, No. 1.

3. BAUER, A. (1965). Crater Method Formulas - A Criticism; Eng. and Min. Journal, Vol. 166, No. 7, July.

4. BAUER, A., HARRIS, G. R., LANG, L, PREZIOSI, P., and SELLECK, D. J., (1965). How IOC Puts Crater Research to Work; Eng. and Min. Journal, Vol. 166, No. 9, September.

5. CLARK, G. B., AND ROLLINS, R. R. (1965): Simplified Explosives Calculations; Eng. and Min. Journal, Vol. 166, No. 6, June.

6. GATES, M. (1964). Blasting Design Criteria; Civil Engineering, Vol. 34, No. 1, January.

7. GRANT, C. H. (1964). Successful Aluminum Slurry Blasts Paved Way for Dow's Explosives Algebra; Eng. and Min. Journal, Vol. 165, No. 8, August.

8. GRANT, C. H. (1964). Simplified Explanation of Crater Method; Eng. and Min. Journal, Vol. 165, No. 11, November.

9. GRANT, C. H. (1965). Design of Open Pits; Proceedings, 7th. Symposium on Rock Mechanics, Penn. State Univ., June.

10. HINO, K. (1959). Theory and Practice of Blasting; Nippon Kayaku Co., Ltd., Asa, Yamaguchi-Ken, Japan.

11. KOCHANOWSKY, B. J. (1957). Principles of Blasting; Univ. of Mo., Sch. of Min. and Met., Rolla, Bulletin, Technical Series No. 94.

12. LANGEFORS, U., and KIHLSTROM, B. (1963). Rock Blasting; John Wiley and Sons, Inc., New York.

13. LEWIS, R. S., and CLARK, G. B. (1964). Elements of Mining; John Wiley and Sons, Inc., 3rd. Ed., N. Y.

14. LIVINGSTON, C. W. (1956). Fundamental Concepts of Rock Failure; Quarterly, Col. Sch. of Mines, Vol. 51, No. 3, November.

15. PEARSE, G. E. (1955) Rock Blasting - Some Aspects on the Theory and Practice; Mine and Quarry Eng. Vol. 21, No. 1 January.

16. SLYKHOUSE, T. E. (1965). Empirical Methods of Correlating Explosive Cratering Results; Proceedings, 7th. Symposium on Rock Mechanics, Penn. State Univ., June.

17. CLARK, L. D., and SALUJA, S. S. (1964). Blasting Mechanics; SME Transactions, Vol. 229.

18. COOK, M. A. (1958). The Science of High Explosives; ACS Monograph 139, Reinhold Publications Co., New York.

19. COOK, M. A., COOK, V. O., and KEYES, R. T. (1965). Behaviour of Rock During Blasting; Proceedings, 7th Symposium on Rock Mechanics, Penn. State Univ., June.

20. NORDYKE, M. D. (1961). On Cratering - A Brief History, Analysis and Theory of Cratering; UCRL Report 6578, August.

21. ASH, R. L. (1961). Drill Pattern and Initiation-Timing Relationships for Multiple-Hole Blasting; Quarterly, Col. Sch. of Mines, Vol. 56, No. 1.

22. LANGEFORS, U., SJOLIN, T., and PEDERSON, A. (1965). Fragmentation in Rock Blasting; Proceedings, 7th. Symposium on Rock Mechanics, Penn. State Univ., June.

23. MATHIAS, A. J. (1964). Pre-Split Blasting; Unpublished M.S. Thesis, Col. Sch. of Mines.

24. ALDRICH, C. A., (1965). A Study of Near Surface Elastic-Anelastic Layers; Unpublished Ph.D. Thesis, Univ. of Mo. at Rolla.

25. AUSTIN, C. F., and PRINGLE, J. K. (1964). Comments on Explosively Formed Fractures in Rock; SME Transactions, Vol. 229.

26. AUSTIN, C. F., PRINGLE, J. K., and FINNEGAN, S. A. (1965). The Fracture and Break-Up of Rock; AIME Preprint No. 65FM63.

27. AUSTIN, C. F., COSNER, L. N., and PRINGLE, J. K. (1965). Shock Wave Attenuation in Elastic and Inelastic Rocks; Proceedings, 7th. Symposium on Rock Mechanics, Penn. State Univ., June.

28. DUVALL, W. I., and ATCHISON, T. C. (1957). Rock Breakage by Explosives; USBM, RI 5356.

29. EWING, W. E., JARDETSKI, W. S., and PRESS, F. (1957). Elastic Waves in Layered Media; McGraw Hill Book Co., Inc., New York.

30. HAAS, C. J. (1964). Coupling Between Unconfined Cylindrical Explosive Charges and Rock; Unpublished D.Sc. Thesis, Col. Sch. of Mines.

31. KOLSKY, H. (1963). Stress Waves in Solids; Dover Publications, Inc., New York.

32. RINEHART, J. S. (1958). Fracturing Under Impulsive Loading; Univ. of Mo., Sch. of Min. and Met., Rolla, Bulletin, Technical Series No. 95.

33. RINEHART, J. S. (1960). Fractures caused by Explosives and Impacts; Quarterly, Col. Sch. of Mines, Vol. 55, No. 4, October.

34. ATCHISON, T. C., and TOURNEY, W. E. (1959). Comparative Studies of Explosives in Granite; USBM, RI 5509.

35. ATCHISON, T. C., and ROTH, J. (1961). Comparative Studies of Explosives in Marble; USBM, RI 5797.

36. ATCHISON, T. C., DUVALL, W. I., and PUGLIESE, J. M. (1964). Effect of Decoupling on Explosion-Generated Strain Pulses in Rock; USBM, RI 6333.

37. ATCHISON, T. C., and PUGLIESE, J. M. (1964). Comparative Studies of Explosives in Limestone; USBM, RI 6395.

38. ATCHISON, T. C., and PUGLIESE, J. M. (1964). Comparative Studies of Explosives in Granite - Second Series of Tests; USBM, RI 6434.

39. DUVALL, W. I., and ATCHISON, T. C. (1950). Vibrations Associated with a Spherical Cavity in an Elastic Medium; USBM, RI 4692.

40. DUVALL, W. I., and PETKOF, B. (1959). Spherical Propagation of Explosion-Generated Strain Pulses in Rock; USBM, RI 5483.

41. DUVALL, W. I., JOHNSON, C. F. , MEYER, A. V. C., and DEVINE, J. F. (1963). Vibrations from Instantaneous and Millisecond-Delayed Quarry Blasts; USBM, RI 6151.

42. HAAS, C. J., and RINEHART, J. S. (1965). Coupling between Unconfined Cylindrical Explosive Charges and Rock; Int. Journal of Rock Mechanics, Mining Science, Vol. 2, Pergamon Press.

43. HOWELL, B. F., Jr. (1964). Birth and Death of a Seismic Pulse; Mineral Industries, Vol. 33, No. 9, Penn. State Univ., June.

44. LEET, D. L. (1960). Vibrations from Construction Blasting; The Explosives Engineer, Jan.-Feb. and Mar.-Apr.

45. MACELWANE, J. B., and SOHON, F. W. (1936). Introduction to Theoretical Seismology: Wiley, New York.

46. NICHOLS, H. R., and HOOKER, V. E. (1962). Comparative Studies of Explosives in Salt; USBM, RI 6041.

47. NICHOLS, H. R. (1964). A Case Study of the Validity of Scaling Laws for Explosion-Generated Motion; USBM, RI 6472.

48. OBERT, L., and DUVALL, W. I. (1950). Generation and Propagation of Strain Waves in Rock, Part I; USBM, RI 4683.

49. QUAN, C. K. (1964). The Characteristics of Radial Strain Propagation Induced by Explosive Impact in Jefferson City Dolomite; Unpublished M.S. Thesis, Univ. of Mo. at Rolla.

50. RAMEZ, M. R. H., and ATTEWELL, P. B. (1963). Shock Deformation of Rocks; Geophysics, Vol. XXVIII, No. 6, December.

51. RUFF, A. W. (1959). The Seismic Wave from Plaster and Drill Hole Explosive Charges; AIME Preprint 59AU109, February.

52. WHITE, J. E., and SENGBUSH, R. L. (1963). Shear Waves from Explosive Sources; Geophysics, Vol. XXVIII, No. 6, December.

53. ASH, R. L., and PEARSE, T. E. (1962). Velocity, Hole Depth Related to Blasting Results; Mining Eng., Vol. 14, No. 9, September.

54. LOVING, F. A. (1965). A Review of Current Blast Strength Theory; Eng. and Min. Journal, Vol. 165, No. 6, June.

55. PEARSE, T. E. (1962). The Influence of Bench Geometry on Blasting Effects for Vertical Cylindrical Charges; Unpublished M.S. Thesis, Univ. of Mo., Sch. of Min. and Met., Rolla.

56. ASH, R. L., RYDLUND, P. H., and YANCIK, J. J. (1965). A Method for Evaluating the Energy Released from Non-Ideal Explosive Reactions; Proceedings, 7th. Symposium on Rock Mechanics, Penn. State Univ., June.

57. ASH, R. L. (1965). The Influence of Petrofabrics on Blast Effects; AIME Preprint No. 65I69.

58. SANDWIN, L. D., and DUVALL, W. I. (1965). A Comparison of Explosives by Cratering and Other Methods; AIME Preprint No. 65AM32.

59. SASSA, K., and ITO, I. (1965). Dynamic Stresses Induced Within Rock in Case of Blasting with One Free Face; Proceedings, 7th. Symposium on Rock Mechanics, Penn. State Univ., June.

60. JOHNSON, J. B. (1962). Small Scale Blasting in Mortar; USBM, RI 6012.

61. JOHNSON, J. B., and FISCHER, R. L. (1963). Effects of Mechanical Properties of Materials on Cratering - A Laboratory Study; USBM, RI 6188.

62. KOCHANOWSKY, B. S. (1961). Theory and Practice of Inclined Drilling for Surface Mining; Quarterly, Col. Sch. of Mines, Vol. 56, No. 1.

63. LANGEFORS, U. (1959). Calculation of Charge and Scale Model Trials; Quarterly, Col. Sch. of Mines, Vol. 54, No. 3, July.

64. PORTER, D. D. (1961). Crater Formation in Plaster of Paris Models by Enclosed Charges; Unpublished M.S. Thesis, Col. Sch. of Mines.

65. Dupont Military Specialties (1964). Bulletin No. ES-58-3B.

66. Ensign-Bickford Company (1960). Primacord Detonating Fuse Catalog, 4th Printing.

67. DEATHERAGE, J. H., JR. (1966). The Development of the Sonic Pulse Technique and Its Comparison with Conventional Static Method for Determining the Elastic Moduli of Rock; Unpublished M.S. Thesis, Univ. of Mo. at Rolla.

68. CLARK, G. B. (1965). Personal Communication.

69. HAAS, C. J., and RINEHART, J. S., (1962). Measurement of Coupling Between Columns of Explosive and Artificial Rocks; NAVWEP Report No. 8055 NOTS TP 3058, November.

70. Handbook of Chemistry and Physics. (1956). Thirty-Eighth Edition, Chemical Rubber Publishing Co., Cleveland, Ohio.

71. Regal Plastic Supply Co. (1963). Catalog. Englewood (Denver), Colorado.

72. WITHEY, M. O., and ASTON, J. (1946). Johnson's Materials of Construction; Eighth Edition, John Wiley and Sons, New York.

VITA

Walter T. Casquino was born on September 7, 1939, in Lima, Peru. He received his primary and secondary education in Lima. He had obtained his college education from the Engineering University of Lima, Peru, receiving a Bachelor of Science Degree in Mining Engineering in 1961.

During 1962 he served as a Junior Engineer at the Yauricocha Mine of the Cerro de Pasco Corporation. From January 1963 to August 1964 he was engaged as a Confederation of British Industries Scholar for the purpose of gaining practical experience in mining and related industries in Great Britain.

In September 1964 he enrolled in the Graduate School of the University of Missouri at Rolla for graduate studies in Mining Engineering.